The Climate Impact of Stratospheric Water Vapour Caused by Aviation Emissions

A Simplified Climate Response Modelling Framework Implemented in OpenAirClim

A. J. Harmsen

Delft University of Technology

TU Delft

The Climate Impact of Stratospheric Water Vapour Caused by Aviation Emissions

A Simplified Climate Response Modelling Framework Implemented in OpenAirClim

by

A. J. Harmsen

to obtain the degree of Master of Science
at the Delft University of Technology,
to be defended publicly on February 26, 2026 at 13:45

Student number:	5060346	
Project duration:	May, 2025 - February, 2026	
Thesis committee:	Prof. dr. V. Grewe	TU Delft | DLR, Supervisor
	Dr. rer. nat. S. Völk	DLR, Supervisor
	Dr. F. Yin	TU Delft, Chair
	Dr. R Merino Martinez	TU Delft, Examiner
Faculty:	Faculty of Aerospace Engineering, Delft	

Cover: Generated with chatGPT

An electronic version of this thesis is available at https://repository.tudelft.nl/.

TU Delft

Abstract

Aviation contributes to anthropogenic climate change not only through CO_2 emissions, but also via non-CO_2 effects, including stratospheric water vapour (SWV). SWV influences the Earth's radiation budget by altering longwave and shortwave radiative fluxes, resulting in a positive radiative forcing. Aviation affects SWV through multiple pathways, including changes in methane oxidation driven by nitrogen oxide emissions, direct emission of water vapour at stratospheric altitudes, hydrogen oxidation, and temperature-driven changes in stratosphere–troposphere exchange. While comprehensive climate chemistry models can represent these processes in detail, their computational cost limits their applicability for rapid scenario analysis.

This thesis develops and evaluates a method to represent aviation-induced changes in stratospheric water vapour within the OpenAirClim (OAC) response model. The novelty of this work lies in the quantification of SWV changes due to methane oxidation within a reduced-form climate response model, enabling fast yet process-consistent scenario analysis. Other potential SWV pathways are assessed but not explicitly implemented due to methodological limitations, overlap with existing OAC modules, or negligible expected impact.

The implementation is verified through consistency checks on fractional release factors, age-of-air distributions, spatial SWV patterns, and mass conservation, and validated against published results. A sensitivity and uncertainty analysis is performed to assess the robustness of the calculated radiative forcing, followed by scenario analyses illustrating the relative magnitude of SWV forcing compared to methane-related effects for different future aviation scenarios. The results demonstrate that aviation-induced reductions in methane lead to a net decrease in SWV and associated radiative forcing, highlighting the importance of including SWV effects for a more complete assessment of aviation's climate impact within simplified climate models.

Contents

List of Figures

List of Tables

Nomenclature

Abbreviations

Abbreviation	Definition
ACARE	Advisory Council for Aviation Research and Innovation in Europe
AoA	Age of Air
ATR	Average Temperature Response
BAU	Business As Usual
CCM	Climate Chemistry Model
CH_4	Methane
CO_2	Carbon Dioxide
CPT	Cold Point Temperature
CurTec	Current Technology
DLR	Deutsches Zentrum für Luft- und Raumfahrt (German Aerospace Center)
ERF	Effective Radiative Forcing
FP2050	Flight Path 2050
FP2050cont	Flight Path 2050 with continous introduction
GWP	Global Warming Potential
GTP	Global Temperature change Potential
H_2	Hydrogen
H_2O	Water
HO_2	Hydroperoxyl
HALOE	Halogen Occultation Experiment
IPCC	Intergovernmental Panel on Climate Change
IRF	Instantaneous Radiative Forcing
ISA	International Stardard Atmosphere
NOAA	National Oceanic and Atmospheric Administration
NO_x	Nitrogen Oxides
O_3	Ozone
OAC	OpenAirClim
OH	Hydroxyl
pdf	Probability Density Function
PMO	Primary Mode Ozone
ppbv	Parts per Billion
ppmv	Parts per Million
RF	Stratospheric Adjusted Radiative Forcing
SSP	Shared Socio-economic Pathway
SWV	Stratospheric Water Vapour

Symbols

Symbol	Definition	Unit
A_{SWV}	Conversion Factor	ppbv ppbv^{-1}
c_v	Coefficient of Variation	-
E	Emission	Tg

Symbol	Definition	Unit
H	Time horizon	yr
m	Mass	kg
M	Molar mass	kg mol^{-1}
p	Pressure level	hPa
P	Production	Tg yr^{-1}
RF	Radiative forcing	W m^{-2}
t	Time	yr
T	Temperature	K or °C
y_{SWV}	Yield of H_2O	mol mol^{-1}
α	Fractional Release Factor	-
θ	Latitude	$^\circ$
λ	Climate Sensitivity Parameter	K(Wm^{-2})$^{-1}$
τ	Lifetime	yr

1

Introduction

Aviation is a rapidly growing sector that contributes significantly to anthropogenic climate forcing with about 3.5% (Lee et al., 2021). While the role of carbon dioxide (CO_2) and nitrogen oxides (NO_x)from aircraft has been widely studied, the influence of stratospheric water vapour (SWV) remains uncertain. SWV affects the Earth's radiation budget by altering both longwave and shortwave fluxes, thereby exerting a positive radiative forcing and amplifying surface warming. This influence is of significant magnitude as a decrease of SWV concentration of 10% slowed global warming with 25% (Solomon et al., 2010). Increases in SWV arise from multiple pathways, including direct emission of water at stratospheric altitudes, methane oxidation, hydrogen oxidation, and temperature-driven changes in stratosphere–troposphere exchange. Quantifying the climate impact of these pathways is essential for understanding the full effect of aviation and for guiding mitigation strategies.

Detailed climate–chemistry models can capture the complex feedbacks involved in SWV formation, but they require extensive computational resources and are impractical for quick scenario analyses. Response models such as OpenAirClim offer a computationally efficient alternative by using pre-computed relationships between emissions and radiative forcing. Incorporating a SWV module into such a response framework enables fast, yet robust assessments of climate impacts of aviation.

This study develops and evaluates methods to represent aviation-induced SWV for the OpenAirClim model. The research aims to quantify the contribution of aviation to global SWV burdens and associated radiative forcing and temperature responses. The results will provide insight into the relative importance of different SWV formation mechanisms.

To guide this investigation, the study addresses the overarching question:

> How can the climate impact of stratospheric water vapour from aviation emissions be quantified and modelled using a simplified climate model?

To answer this research question, first, some literature is discussed in chapter 2. Second, the methodology is described in chapter 3. Third, the methodology is verified and validated in chapter 4. Fourth, a sensitivity study and uncertainty analysis are done in chapter 5, Fifth, a scenario analysis is done in chapter 6, and finally, conclusions and recommendations form future work are stated in chapter 7.

2

Literature Review

In recent years, the significance of stratospheric water vapour (SWV) as a contributor to climate change has gained increasing attention, particularly in the context of aviation emissions, as aviation introduces both direct and indirect sources of water vapour into the stratosphere. Understanding the climate impact of aviation-induced SWV requires an in-depth view of multiple atmospheric processes.

This chapter provides a comprehensive review of the relevant literature on the climatic effects of SWV with a focus on aviation. Section 2.1 outlines the key physical metrics used to quantify climate impact, such as radiative forcing (RF), surface temperature change (ΔT_s), and several climate metrics. Section 2.2 discusses how aviation emissions contribute to SWV, including pathways via transport from the troposphere, methane (CH_4) oxidation, direct water emissions, and hydrogen (H_2) oxidation. In section 2.3, the broader climatic implications of SWV are discussed, focusing on its contribution to radiative forcing. Finally, section 2.4 introduces the OpenAirClim response model and evaluates how it can be adapted to simulate the impact of aviation-related SWV on global climate.

By combining insights from multiple studies, this chapter aims to establish a theoretical foundation for the implementation and evaluation of an SWV module within the OpenAirClim model.

2.1. Climate Impact

To compare the impact of various emissions on the climate, several key quantities are defined. These provide insight into both the immediate and long-term effects of emissions. Different types of radiative forcing, which is closely related to the actual emissions, and the resulting steady-state surface temperature (ΔT_s) are discussed in subsection 2.1.1. In addition, the climate metrics Global Warming Potential (GWP), Global Temperature change Potential (GTP), and Average Temperature Response (ATR), which offer more indirect assessments, are introduced in subsection 2.1.2.

2.1.1. Radiative Forcing and Surface Temperature Change

Radiative forcing is a key concept used to quantify the climate impact of different atmospheric species. It is defined as:

> "The change in the net, downward minus upward, radiative flux (expressed in W m^{-2}) due to a change in an external driver of climate change."(IPCC, 2001)

In essence, radiative forcing measures the imbalance between incoming solar radiation and outgoing infrared radiation. A positive RF indicates that more energy is entering the Earth system than leaving, leading to a warming effect. On the other hand, a negative RF implies that more energy is leaving than entering, resulting in a cooling effect. When the net flux is balanced, RF equals 0 W m^{-2}, and there is no net energy gain or loss.

The IPCC (2013) also distinguishes between different types of radiative forcing: Instantaneous Radiative Forcing (IRF), Effective Radiative Forcing (ERF), and stratospherically adjusted Radiative Forcing (RF).

IRF refers to the immediate change in top-of-atmosphere radiative flux caused by a perturbation, before any atmospheric temperature adjustments or feedbacks occur.

ERF incorporates rapid atmospheric adjustments, such as changes in water vapour, cloud cover, and atmospheric temperature, while keeping the surface temperature constant. ERF is defined as:

> "We term a forcing that accounts for rapid adjustments the effective radiative forcing (ERF). Conceptually, ERF represents the change in net TOA (Top Of Atmosphere) downward radiative flux after allowing for atmospheric temperatures, water vapour and clouds to adjust, but with global mean surface temperature or a portion of surface conditions unchanged."(IPCC, 2013)

RF is defined as the change in net radiative flux at the top of the atmosphere after allowing the stratospheric temperature to adjust to radiative equilibrium, while keeping tropospheric temperatures and surface conditions fixed (IPCC, 2013).
This adjustment accounts for the rapid thermal response of the stratosphere, which typically occurs on timescales of weeks to months. It is particularly relevant for forcing agents that directly perturb the stratosphere, such as stratospheric ozone, aerosols, and stratospheric water vapour. Allowing the stratosphere to adjust removes artificial radiative imbalances that would otherwise arise from purely instantaneous forcing calculations.
RF generally shows a more consistent relationship with long-term surface temperature change than instantaneous RF for stratospheric perturbations. However, unlike ERF, it does not include rapid adjustments in the troposphere, such as changes in water vapour, clouds, or lapse rate. For this reason, ERF is considered the most comprehensive forcing metric, while RF remains a useful intermediate metric, particularly in studies focusing on stratospheric processes, including aviation-induced climate effects.

Both RF and ERF are widely used in climate modelling and assessment reports to evaluate the effects of different atmospheric species over time.

Radiative forcing can be used to estimate the change in steady-state global mean surface temperature (ΔT_s) using the following linear relationship:

$$\Delta T_s = \lambda \cdot RF \tag{2.1}$$

Here, λ is the climate sensitivity parameter (in units of K(W m^{-2})$^{-1}$), and RF is the radiative forcing in Wm^{-2}. According to the IPCC (2013), a commonly used estimate for λ is 1.0 ± 0.5 K(W m^{-2})$^{-1}$) for a doubling of CO_2, based on the mean output of approximately 30 climate models.

2.1.2. Climate Metrics

To quantify and communicate the relative and absolute contributions of emissions to climate change, climate metrics are defined. In this section, three of those metrics will be discussed. These are: Global Warming Potential (GWP), Global Temperature change Potential (GTP) and the Average Temperature Response (ATR).

GWP

Global Warming Potential (GWP) was first introduced in the First IPCC Assessment Report (Houghton et al., 1990), the GWP was originally presented as a simplified tool to illustrate the complexities in comparing greenhouse gas emissions. At the time, it was explicitly noted that there was no universally accepted methodology for combining the various influencing factors into a single metric. GWP provides an indirect measure of the total energy added to the climate system by a given gas relative to CO_2. However, it does not directly correspond to temperature change or other climate impacts.

The GWP is defined as the time-integrated RF due to a pulse emission of a given component, relative to a pulse emission of an equal mass of CO_2 (Myhre et al., 2013). The formula used to calculate GWP is stated in Equation 2.2. Where $RF_{\text{spec}}(t)$ is the RF of the species of interest as a function of time, $RF_{\text{CO}_2}(t)$ is the RF from an equal mass of CO_2 and H is the time horizon that is used.

The GWP is generally integrated over timescales of 20, 50 and 100 years. The choice of this timescale is of large influence of the value of the GWP due to the lifetime of certain species. When a species has a short lifetime. the GWP20 will be much higher than the GWP100. In general, GWP100 is set as standard GWP. This decision was made to standardize and facilitate easy comparisons, although there is no scientific argument for this choice.

Further complexities arise from decisions regarding the background atmospheric state, the treatment of indirect effects and feedbacks, and the assumed radiative efficiencies. These factors contribute to uncertainties in GWP values. Due to these uncertainties and the high dependency on the timescale, GWP must be used carefully such that it will not be misused.

$$\text{GWP} = \frac{\int_0^H RF_{\text{spec}}(t)\,dt}{\int_0^H RF_{\text{CO}_2}(t)\,dt} \tag{2.2}$$

GTP

The Global Temperature change Potential (GTP) is a climate metric designed to estimate the change in global mean surface temperature at a specific point in the future due to an emission pulse of a given greenhouse gas, relative to the impact of CO_2. It is calculated using the formula stated in Equation 2.3, where ΔT^H_{spec} Is the temperature change due to a species at time H and $\Delta T^H_{CO_2}$ is the temperature change due to CO_2 at time H. GTP is first introduced by Shine et al. (2005), GTP differs fundamentally from the more commonly used GWP. While GWP integrates the radiative forcing of a gas over a given time horizon, GTP focuses on the temperature change at a chosen future year.

GTP captures the physical processes that affect how emissions translate into temperature change. These include climate sensitivity, the transfer of heat between the atmosphere and the deep ocean, and the atmospheric adjustment time scales specific to each gas. By incorporating such processes, GTP provides a more direct measure of how emissions will influence future global temperatures, particularly for long-lived and short-lived emissions.

One of the key advantages of GTP is that it links emissions to a more policy-relevant outcome: the expected temperature change at a target year. This makes it especially useful for climate strategies aiming to stay within specific temperature limits, such as the 1.5°C or 2°C thresholds outlined in the Paris Agreement. Additionally, GTP can be calculated for both pulse emissions and sustained emissions over time.

However, the metric also comes with limitations. GTP values are sensitive to the choice of time horizon and depend heavily on assumptions about climate sensitivity and ocean heat uptake. These dependencies introduce greater uncertainty compared to GWP, especially for short-lived climate forcers. Furthermore, GTP values can vary depending on how feedbacks and indirect effects are accounted for in the background atmosphere.

Despite its complexity and uncertainty, GTP offers a more direct link between emissions and their long-term temperature impacts, making it a valuable complement to GWP in climate policy analysis.

$$\text{GTP} = \frac{\Delta T^H_{\text{spec}}}{\Delta T^H_{CO_2}} \tag{2.3}$$

ATR

The Average Temperature Response (ATR) is a more recently proposed climate metric intended to represent the mean global surface temperature change over a selected time horizon following a pulse emission of a given greenhouse gas, relative to that of an equal mass of CO_2. It was highlighted by Megill et al. (2024) as a metric that combines aspects of both the Global Warming Potential (GWP) and the Global Temperature change Potential (GTP), while offering a clearer link to the cumulative thermal impact of emissions and is the most appropriate climate metric for aircraft design and aviation policy according to Megill et al. (2024).

Unlike GWP, which integrates radiative forcing over time, or GTP, which evaluates the temperature change at a single future point, ATR averages the temperature response across the entire chosen

horizon. Mathematically, ATR is defined as the mean of the instantaneous global mean surface temperature change for a specific species $\Delta T_{\text{spec}}(t)$ over a horizon H (see Equation 2.4):

$$\text{ATR} = \frac{1}{H} \int_0^H \Delta T_{\text{spec}}(t) dt \tag{2.4}$$

The choice of H, often 20, 50, or 100 years, strongly influences the resulting value, especially for gases with short atmospheric lifetimes. Short-lived climate forcers will exhibit high ATR values for short horizons, reflecting their sharp but transient warming effect, while long-lived gases show a more sustained response.

ATR's key strength lies in its direct physical interpretation: it quantifies the average global temperature impact over a policy-relevant period, which is useful when assessing cumulative temperature exposure or near-term warming commitments. This makes it particularly appealing for evaluating mitigation strategies aimed at limiting mid-century warming.

However, as with GWP and GTP, ATR depends on assumptions about climate sensitivity, ocean heat uptake, and background atmospheric conditions. Uncertainties in these parameters propagate into the calculated metric. Moreover, because ATR represents an average rather than a single peak or total energy input, its policy relevance differs from that of GTP (which targets a specific temperature year) or GWP (which targets cumulative radiative forcing).

Despite these caveats, ATR offers a complementary perspective for climate policy: it provides a scientifically grounded, yet relatively intuitive, measure of the average thermal effect of emissions over a chosen timeframe, bridging the gap between integrated forcing and end-point temperature metrics.

2.2. Impact of Aviation Emissions on SWV Concentration

SWV can originate from different sources. Four main sources are discussed in this section. The possible sources are: water vapour transport from the troposphere (subsection 2.2.1), oxidation of CH_4 (subsection 2.2.2), direct emission of water vapour into the stratosphere (subsection 2.2.3), and oxidation of H_2 (subsection 2.2.4).

2.2.1. Water Vapour Transport from the Troposphere

Transport of water vapour from the troposphere to the stratosphere is dependent on multiple factors, like the Brewer-Dobson circulation through the tropics, extratropical transport, volcanic eruptions, deep convection, and meteorological events like the El Niño southern oscillation and the quasi-biennial oscillation (Dessler et al., 2013; Diallo et al., 2022).

The main transport from H_2O to the upper stratosphere happens due to the Brewer-Dobson circulation, which transports H_2O from the tropical troposphere upwards to the stratosphere (Dessler et al., 1995). In the stratosphere, air moves due to this circulation from the tropics to the poles. The amount of H_2O that is transported in this way is largely dependent on the cold point tropopause (CPT), which is the coldest point the air parcel experiences, influencing the specific humidity of that air parcel. (Revell et al., 2016).

Fueglistaler et al. (2005) estimates an H_2O mixing ratio of air entering the stratosphere of 3.5 ppmv for the period 1979-2001. However, Gettelman et al. (2010) estimates the CPT to warm over the coming century with about 1 K per century, leading to an increase in H_2O concentration of 0.5-1 ppmv per century. Randel and Park (2019) estimates that the concentration of H_2O will increase by 0.5 ppmv per K CPT warming, they also show that in the tropical stratosphere, the CPT temperature and SWV concentration are highly correlated. At higher altitudes, the correlation is less due to methane oxidation causing SWV as well. The correlation is also lower in the extratropical lower stratosphere, as extratropical transport plays a larger role there. Nowack et al. (2023) estimates the dependency of H_2O entering the stratosphere relative to global temperature increase to be 0.31 ± 0.39 ppmv K^{-1}. This is lower than the value from Gettelman et al. (2010), but this value is related to global temperature increase and the value from Gettelman et al. (2010) is related to warming of the CPT.

Dessler et al. (2013) show that not only temperature but also the quasi-biennial oscillation and the strength of the Brewer-Dobson circulation have an effect on the H_2O entering the stratosphere, but these effects are smaller than the influence of the CPT according to Randel and Park (2019). In the lower stratosphere, the H_2O transport is mostly dominated by transport through the extratropical tropopause, as the extratropical tropopause is much warmer than the tropical tropopause, higher concentrations of H_2O can be found here, in the order of tens of ppmv. (Dessler et al., 1995)

Aviation emissions do not directly influence the H_2O transport to the stratosphere. However, aviation does contribute to global warming and therefore also the warming of the CPT. Through this indirect pathway, aviation indirectly causes the transport to increase.

2.2.2. CH_4 Oxidation

Aviation emissions contain nitrogen oxides (NO_x) due to the reaction of nitrogen with oxygen under the high pressure and temperature in the turbine (Schumann, 1997). When this NO_x is emitted in the atmosphere, it will react with hydroperoxyl (HO_2) to form hydroxyl (OH) radicals. An increase in OH radicals will fasten the dissimilation of CH_4, resulting in a lower CH_4 concentration (Rieger, 2018). When CH_4 reacts with OH, H_2O is formed (Equation 2.5 obtained from Rieger (2018)). When the CH_4 concentration goes down due to aviation emissions, the resulting SWV concentration will also go down, as there is less CH_4 in the stratosphere to oxidize.

$$\mathrm{CH_4 + OH + O_2 \rightarrow CH_3O_2 + H_2O} \tag{2.5}$$

The relations between aviation emissions and the methane concentration are well studied. A proven method to determine the global averaged methane concentration is the method of Rieger (2018). This method, referred to as the tagging method, calculates the CH_4 concentration change by taking the effect of OH on the lifetime into account.

How this change in CH_4 influences the SWV is explained by Revell et al. (2016). Revell et al. (2016) also discuss a formula that links the methane concentration to the SWV concentration and can be found in Equation 2.6 (Austin et al., 2007; Oman et al., 2008).

$$\mathsf{H_2O}(\theta, p, t) = \mathsf{H_2O}|_{\mathsf{e}}(t - AoA) + 2[\mathsf{CH_4}|_0(t - AoA) - \mathsf{CH_4}(\theta, p, t)], \tag{2.6}$$

In Equation 2.6, H_2O is determined for each latitude (θ), pressure level (p) and time (t), $H_2O|_e$ is the tropical (10° North–10° South) water vapour concentration at 70 hPa, AoA is the age of air (dependent on θ, p and t), $CH_4|_0$ is the tropical methane concentration at 150 hPa, and CH_4(θ, p, t) is the methane concentration at the location and time, the H_2O concentration is determined. The first term in Equation 2.6 ($H_2O|_e(t - AoA)$) represents water vapour concentrations entering the stratosphere, the second term represents the contribution to SWV from methane oxidation. The age of air for each latitude, pressure and time is included because for a given parcel of air, entry into the stratosphere will have occurred at an earlier time (depending on where the parcel of air is), and the amount of methane that is oxidised depends on the time since that parcel of air resided in the troposphere (Austin et al., 2007). In Equation 2.6 the assumption is made that every CH_4 molecule will form 2 H_2O molecules (le Texier et al., 1988). However, other studies have found that this 2 is not always fixed, as CH_4 could also dissimilate to H_2 or react with other species like chlorine (le Texier et al., 1988). Frank et al. (2018) did a thorough research and found that the amount of H_2O produced by one CH_4 is heavily dependent on pressure level and varies in value between 1.4 and 2.2.

Other papers estimate the global SWV production is by using the CH_4 sink. When willing to estimate the global averaged SWV production from CH_4 oxidation, one can fall back on Equation 2.7. Where $\Delta m_{SWV_{CH_4}}$ is the change in SWV mass due to methane oxidation, $\Delta m_{CH_{4loss}}$ is the change stratospheric loss of methane mass due to oxidation of methane, and M_{CH_4} and M_{SWV} are the molar masses of methane and water, respectively. As essentially every CH_4 molecule will form approximately 2 water molecules, to relate it to masses, the molar mass of both species is incorporated (Revell et al., 2016). To use Equation 2.7 to estimate the change in SWV due to CH_4 oxidation, one has to estimate the change in stratospheric loss of CH_4. Multiple sources estimate the annual loss of CH_4. Winterstein and Jöckel (2021) estimates the stratospheric sink to be 8% of the total CH_4 sink. They base their

values on IPCC (2013). IPCC (2013) based their values on Kirschke et al. (2013) where there are values for stratospheric methane loss and total methane loss averaged over decades. The estimates of Kirschke et al. (2013) have significant variance, going from 8.4%-11.7% for different decades and the values themselves have a spread of 3.3%-13.4%. Although this variance is high, 8% is deemed a proper average (Winterstein & Jöckel, 2021) and is in accordance with estimates of IPCC (2001), Stevenson et al. (2006), and Voulgarakis et al. (2013). The total global CH_4 loss can be estimated with the global averaged CH_4 concentration, [CH_4], and the estimated CH_4 lifetime, τ_{CH_4}, and the relation stated in Equation 2.8, where m_{atm} is the atmospheric mass, M_{air} is the molar mass of air and M_{CH_4} is the molar mass of CH_4.

$$\Delta m_{SWV_{CH_4}} \approx 2\Delta m_{CH_{4loss}} \cdot \frac{M_{CH_4}}{M_{SWV}} \tag{2.7}$$

$$CH_{4loss} = m_{atm} \cdot \frac{[CH_4]}{\tau_{CH_4}} \cdot \frac{M_{air}}{M_{CH_4}} \tag{2.8}$$

The paper of Myhre et al. (2007) also gives insights into the amount of SWV due to CH_4 oxidation. They quantified the increase of SWV resulting from CH_4 oxidation over three historical intervals: 1750–2000 (entire industrial era), 1950–2000 (period including more than half of the anthropogenic CH_4 increase), and 1979–2000 (for which satellite data is available). For these three intervals, a SWV distribution dependent on both latitude and altitude is made and displayed in their figure 2.

2.2.3. Direct H_2O Emission

When fuel is combusted in the engine, the two main components exhausted are CO_2 and H_2O. When the aircraft flies at stratospheric altitudes, this H_2O is SWV. When an aircraft flies in the troposphere, this H_2O has little effect on the SWV concentration as the troposphere is relatively humid and the additional H_2O is marginal and does not influence the transport as this is limited by the CPT (subsection 2.2.1) (Dessler et al., 2013).

To estimate the amount of SWV due to direct emission of aircraft, one has to know the boundary between the troposphere and the stratosphere, also known as the tropopause. Emissions that happen above the tropopause are in the stratosphere, emissions below the tropopause are in the troposphere.

Hoffmann and Spang (2022) have investigated the tropopause location using ERA5 data. From this data, it can be seen that the tropopause changes altitude for different latitudes and different seasons. There is also a variation between years. This makes estimating the exact tropopause location for future scenarios hard. However, estimates could be made.

Comparisons of aircraft cruise altitudes with mean tropopause heights have led to estimates for stratospheric release of 20-40% of total emissions (Penner et al., 1999). Wilcox et al. (2012) did research to the amount of H_2O that is emitted in the stratosphere. They show in their figure 3 that the tropopause location causes different percentages of the emissions to be in the stratosphere. For the North Atlantic Flight Corridor, this fraction varies from 40% in June to 65% in March. Globally, the fraction varies between 15 and 30% for the year 2006, with an average of 25%. It should be noted that current aviation flies mostly between 9-13 km altitude, so if the emissions are in the stratosphere, the emissions are only in the lower parts of the stratosphere close to the tropopause.

2.2.4. Hydrogen Leakages

Hydrogen (H_2) is not directly emitted by aviation. However, when changing to a more sustainable future, H_2 will play a key role (Gunter, 2024; Warwick et al., 2022). When more H_2 will be produced and used, more will end up in the atmosphere due to leakages (Skeie et al., 2025). In this section, the effect of leakages of hydrogen on the SWV concentration will be considered.

H_2 emissions can lead to the formation of SWV. There are two ways in which H_2 influences the SWV concentration (Paulot et al., 2021). The most direct mechanism is by oxidation of H_2 with OH to form H_2O. When this happens in the stratosphere, SWV will be formed. A method to estimate this is by the use of Equation 2.9 (Gunter, 2024). Where $\Delta[SWV]_{H_2}$ is the change in SWV concentration due to H_2,

A_{SWV} is a conversion factor of 0.3 $ppb_{SWV} ppb_{H_2}^{-1}$ (Warwick et al., 2022), and $\Delta[H_2]$ is the change in global H_2 concentration. However, Gunter (2024) concludes that this method might be oversimplified.

$$\Delta[SWV]_{H_2} = A_{SWV} \cdot \Delta[H_2] \tag{2.9}$$

The other pathway is dependent on the CH_4 concentration, as when H_2 reacts with OH in the troposphere, this will result in a lower OH concentration. Due to this lower OH concentration, the tropospheric CH_4 concentration will rise as the main sink of CH_4 is the reaction with OH. This higher CH_4 concentration will cause more SWV as explained in subsection 2.2.2. The way Warwick et al. (2022) handle this CH_4 induced change in SWV is by applying a scaling factor of 0.15 $\pm$ 70% on the radiative forcing of CH_4 caused by a change in H_2 concentration, so no direct SWV concentration changes are calculated. Gunter (2024) estimates the CH_4 induced SWV concentration change due to H_2 using a neural network. The results obtained by Gunter (2024) are in the same range as other models discussed by Sand et al. (2023).

2.3. Impact of SWV on RF

To determine the impact of SWV on climate change it is wise to first look at the change in RF as that directly relates to a change in concentration (subsection 2.1.1). There are different publications investigating the RF caused by SWV.

Myhre et al. (2009) looks into the RF for an instantaneous SWV concentration change from 3.0 to 3.7 ppmv. They have compared different models and the net SWV RF they obtain is 0.245 or 0.262 Wm^{-2} depending on the averaging they use, both values differ not significantly and are both within the error margins of the models, leading to a sensitivity of 0.35 or 0.37 Wm^{-2} $ppmv_{H_2O}^{-1}$

In Myhre et al. (2007), the change in forcing of SWV due to changes in CH_4 concentration over certain periods is investigated. They found that the changes in RF caused by SWV formed by CH_4 oxidation are 0.083 Wm^{-2} for the period 1750-2000, 0.050 Wm^{-2} for the period of 1950-2000, and 0.016 Wm^{-2} for the period of 1979-2000 (see Table 1 in Myhre et al. (2007)). Which generalizes to around 15-20% of the forcing directly due to methane for the same periods.

Pletzer (2024) discusses another method to determine the RF due to SWV, he looks at the total H_2O mass perturbation above the tropopause due to aviation emissions. He relates that H_2O mass perturbation to a net RF. He comes to similar results as Grewe et al. (2014) but has extended the model from Grewe et al. (2014) for more accuracy when the H_2O emission takes place at higher altitudes in the stratosphere. He modelled multiple emission scenarios and estimated a polynomial fit (Equation 2.10).

$$y = ax^2 + bx + c \tag{2.10}$$

In Equation 2.10, y is the net RF in mWm^{-2}, x is the H_2O perturbation above the tropopause in Tg, a, b, and c equal -0.00088, 0.47373, and -0.74676 $mWm^{-2}Tg^{-1}$ respectively. The results are validated for total aircraft fleet emissions and are also valid for different initial emissions species, i.e., for NO_x, H_2O and H_2.

Lee et al. (2021) estimate the RF and ERF for aviation emissions for the period of 2000 until 2018 based on other literature. They found an increase in SWV due to emissions of H_2O and a decrease in SWV due to decreased CH_4 oxidation. The ERF and RF related to these changes can be found in Table 2.1, where the values include an error margin and are dependent on the magnitude of the emission.

Table 2.1: Values for the changes in RF and ERF due to changes in SWV from aviation emissions (Lee et al., 2021).

	ERF	RF	Unit
SWV increase	0.0052 ± 0.0026	0.0052 ± 0.0026	$mW\,m^{-2}\,(Tg(H_2O)\,yr^{-1})^{-1}$
SWV decrease	-2.8 ± 1.0	-2.4 ± 0.9	$mW\,m^{-2}\,(Tg(N)\,yr^{-1})^{-1}$

2.4. Modelling using OpenAirClim

Different models can be used to model climate impact of emissions. A distinction can be made between Climate Chemistry Models (CCM) and simplified models. A CCM first calculates all the atmospheric

changes caused by a certain emission and then relates these atmospheric changes to changes in RF. A simplified model, like a response model, does not calculate exactly all atmospheric changes but uses simplified ways to directly relate an emission to a RF. This is visualized in Figure 2.1 from Völk et al. (2026), where it can be seen that the response model working with look-up tables skips the step of calculating all atmospheric changes compared to the traditional CCM approach. This has significant benefits in computational time. Where response models take seconds to run on a desktop computer, CCMs require up to several weeks to run (Völk et al., 2026). This makes response models very useful for situations where multiple simulations are required. The response model used in this thesis is OpenAirClim (OAC) developed by the German Aerospace Center (DLR) and based on AirClim developed by Grewe and Stenke (2008).

The core of OpenAirClim's methodology is response modelling, which applies response surfaces derived from detailed CCMs. These surfaces are used as look-up tables and represent non-linear relationships between emissions and radiative forcing. OAC processes emission inventories in four dimensions, longitude, latitude, altitude (pressure level), and time. This is done to provide a precise evaluation of the climate impact of aviation. In this way, emissions of species can be linked to the proper look-up table and related to a RF.

The species that OAC can handle are the emissions CO_2, NO_x and H_2O. As NO_x is an indirect forcer, its effects on O_3, CH_4 and Primary Mode Ozone (PMO) are taken into account as well. Furthermore, there is a module in OAC to calculate the climate impact of contrails. The way the RF for these different species is calculated differs for each species.
For CO_2, first, the difference in concentration is calculated due to the emission. Next, the change in concentration is related to a RF based on the selected method from literature (default is the method from Etminan et al. (2016), but different methods are included in OAC as well). The location of the emission of CO_2 is not considered, as CO_2 has a very long lifetime and therefore perfect mixing can be assumed. Species for which emission location is not important are also referred to as 0D.
For the H_2O emissions, the location is of importance. This species is referred to as 2D as the latitude and pressure level dimensions are of importance. The emitted H_2O is compared with the look-up table for H_2O and a RF value is obtained.
For the products from the NO_x emission (CH_4 and O_3) the methods are slightly different. The method for O_3 relates closely to that of H_2O as O_3 is also 2D, the additional step that must be made is to convert the NO_x emission to an O_3 concentration change. A specific look-up table is generated to relate the O_3 RF to NO_x emissions.
For CH_4, the method is different as it makes use of the tagging method described by Rieger (2018). In this method, a NO_x emission is related to the lifetime of CH_4 and that lifetime is related to a global CH_4 concentration. Next, the RF due to this concentration change can be calculated using the method described by Etminan et al. (2016). This is possible as CH_4 has a lifetime long enough that the emission location is not of importance.
The last species that can also be modelled in OAC is Primary Mode Ozone (PMO). The RF due to PMO is calculated based on a linear relation between the PMO RF and the RF due to CH_4. When the RF due to CH_4 is obtained, the RF due to PMO is calculated as well.
One species that is not included in OAC is SWV. This thesis will lay a foundation for the implementation of SWV in OAC.

After the RF for a certain emission is determined, it can be related to a temperature chance and other climate metrics (GWP, GTP, ATR) such that the effects of the emission can be reported and compared with other scientific work.

OAC is designed to simulate global emissions on a corresponding timescale (the smallest resolution is a year). This is ideal to investigate the impact of new aviation technologies on the climate. For instance, when fuels other than the traditional kerosene are used.

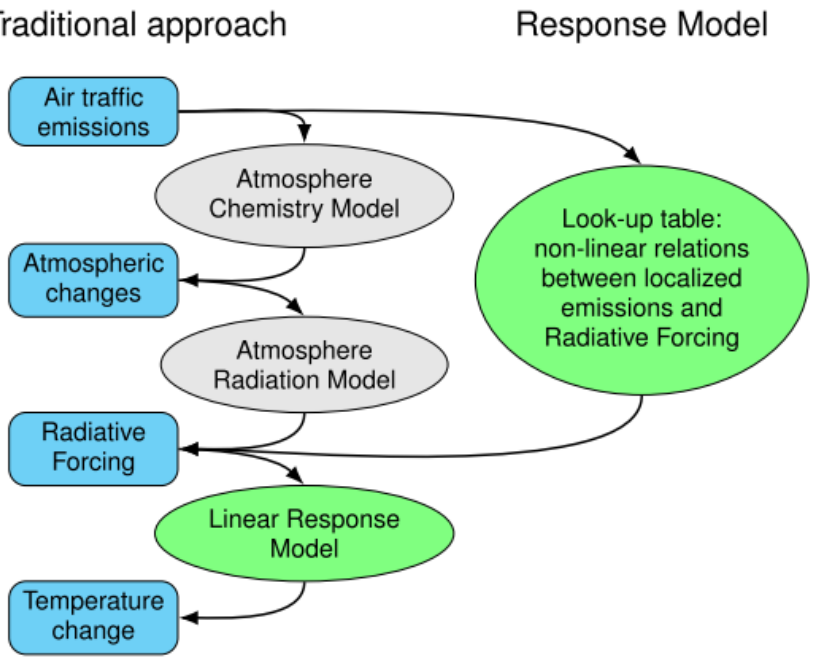

Figure 2.1: Schematic overview of the approach using climate chemistry modelling and using response modelling used by the OpenAirClim Framework (Völk et al., 2026)

3

Methodology

SWV originates from several different atmospheric processes. This chapter describes the methods used to represent each of these sources within OAC, if it is deemed a valuable addition to the model. In section 3.1, the method for the implementation of SWV production from CH_4 oxidation is outlined. Section 3.2 presents the approach used to account for SWV arising from direct emissions. The contribution of transport of tropospheric water vapour to the stratosphere is discussed in section 3.3. Section 3.4 details the method applied to estimate the contribution of H_2 oxidation, mainly originating from H_2 leakages. Consequently, this thesis implements a modelling approach only for SWV formation driven by CH_4 oxidation, while other potential sources of aviation-induced SWV are not implemented due to their secondary contribution, high uncertainty, or incompatibility with the scope and structure of the present study.

3.1. CH_4 Oxidation Method

SWV is formed during the oxidation of CH_4. Aviation emissions influence this process as the NO_x emissions of aircraft cause the OH concentration to increase, thereby accelerating the dissimilation of CH_4 and consequently lowering the global CH_4 concentration.

To implement this adjustment within the OAC framework, a two step approach is taken. This approach consist of first calculating the SWV perturbation mass due to CH_4 oxidation, and second, this mass is related to a RF.

The impact of changes in CH_4 concentrations on SWV concentrations is determined using the parameterisation originally derived by Austin et al. (2007) and Oman et al. (2008) and later adapted by Hegglin et al. (2014). Austin et al. (2007) state that the total concentration of water vapour at a certain location (pressure level p and latitude θ) in the stratosphere at a certain time (also referred to as SWV(θ, p, t)) is dependent on the H_2O entering the stratosphere lagged by the age-of-air ($H_2O|_e(t - AoA)$) and the amount of CH_4 that is oxidized ($CH_4|_0(t-AoA) - CH_4(\theta, p, t)$) the total amount of SWV is estimated using Equation 2.6. The entering concentration is determined at the tropical tropopause. In this equation, the assumption is made that each CH_4 molecule produces 2 water molecules (le Texier et al., 1988) as this factor 2 is widely used in literature. It should be noted that in reality this factor would be dependent on altitude (Frank et al., 2018).

Equation 2.6 can be rewritten using the fractional release factor α. α is defined as shown in Equation 3.1 by Hegglin et al. (2014). Where $\mathrm{CH_4}$(p, θ, t) corresponds to the methane concentration at a given location and time in the stratosphere and $CH_4|_e(t-AoA)$ is the amount of CH_4 entering the stratosphere lagged by the AoA.

$$\alpha(\theta, p) = \frac{CH_4|_e(t - AoA) - CH_4(\theta, p, t)}{CH_4|_e(t - AoA)} \tag{3.1}$$

To calculate the change in SWV due to methane oxidation (ΔSWV) based on the change in methane

entry concentration, with corresponding time lag ($\Delta CH_4|_e$(t-AoA)), Equation 2.6 and Equation 3.1 can be combined as is done in the publication of Hegglin et al. (2014). In this new equation, the effect of the water vapour transported to the stratosphere is not included, as the focus is solely on the SWV formed by CH_4 oxidation. This results in Equation 3.2.

$$\Delta SWV(\theta, p, t) = 2\alpha(\theta, p)\Delta CH_4|_e(t - AoA) \tag{3.2}$$

Equation 3.2 will be implemented in OAC. To achieve that, α must be determined. This is done based on a reference scenario, from which α can be obtained. α is assumed to remain constant over time and is therefore not time dependant. This is valid because the fractional release is dependent on circulation and the background OH concentration, which are assumed to remain constant (Hegglin et al., 2014).

The reference scenario used to determine α is based on the Halogen Occultation Experiment (HALOE) data. Specifically, the HALOE zonal mean vertical CH_4 profile averaged over the period from October 1991 to 1999, as reported by Myhre et al. (2007). This distribution is displayed in Myhre et al. (2007) Figure 1. The period in the 1990s is chosen as during the 1990s the CH_4 levels are relatively steady, so the time lag becomes of minor importance. Using this observed profile, together with the average methane entry value over this period of 1772 ppbv determined by the National Oceanic and Atmospheric Administration (NOAA)[1], a vertical α profile can be estimated.

The AoA can be determined using an empirical relationship between α and AoA established by Hegglin et al. (2014). Hegglin et al. (2014) described the relation between α and AoA by a third-order polynomial (Equation 3.3). Based on this relationship, an AoA profile is generated. Since the smallest temporal resolution in OAC is one year, the calculated AoA values are rounded to integer years and the corresponding locations based on altitude and latitude are lagged accordingly.

$$AoA = 0.3 + 15.2\alpha - 21.2\alpha^2 + 10.4\alpha^3 \tag{3.3}$$

Using the formulas explained above, the ΔSWV can be determined for each location for a given CH_4 entry concentration. The resulting change in total SWV mass, Δm_{SWV}, can be computed by summing over all locations. This is done by determining the SWV mass at each location using the air mass of the corresponding location, based on the International Standard Atmosphere (ISA) ($m_{air}(\theta, p)$), and the molar masses of air (M_{air}) and water (M_{H_2O}). Summing this over the whole range of pressure levels and latitudes gives a total SWV mass (Equation 3.4). This total SWV mass will be used to calculate the associated RF.

$$\Delta m_{SWV}(t) = \sum_{\theta} \sum_{p} \Delta SWV(\theta, p, t) m_{air}(\theta, p) \frac{M_{H_2O}}{M_{air}} \tag{3.4}$$

The RF of SWV is determined with the use of the relation found by Pletzer (2024) in his figure 7.17 and stated in this thesis as Equation 2.10. Using Equation 2.10, a change in SWV mass can be directly related to a change in RF. Combining the two steps, a total RF from SWV caused by CH_4 oxidation can be determined using OAC.

In OAC, the value of global CH_4 change due to aviation emissions is already calculated. When combining this CH_4 change with the total amount of SWV caused by CH_4 in the stratosphere is determined. It is important to note that due to aviation emissions, the CH_4 concentration will become lower and therefore the amount of SWV also becomes lower. This assumption is valid as long as the CH_4 concentrations do not go below pre-industrial values (which is very unlikely in the upcoming centuries) as in those scenarios the data of Myhre et al. (2007) might not be sufficient as other non-linear effects might play a role. Furthermore, Pletzer (2024) derived the relation from simulation data, but this data has a range until a perturbation magnitude of 160 Tg. Therefore, for perturbations higher than 160 Tg, the relation in Equation 2.10 will not be valid. Also, due to the fit to the simulated data, at small increases in SWV (less than 1.6 Tg), the sign is negative. Since this behaviour does not reflect atmospheric chemistry, for values smaller than 1.6 Tg, the RF is set to 0 W m^{-2} instead.

[1] https://gml.noaa.gov/webdata/ccgg/trends/ch4/ch4_annmean_gl.txt, accessed 05-12-2025

3.2. Direct Emission Evaluation

This section assesses the effects of direct H_2O emissions into the stratosphere and justifies the decision not to develop a model that explicitly accounts for their influence on SWV.

In OAC, there is already a module to calculate the radiative forcing of emitted water vapour. It does not differentiate between which part is tropospheric and which part is stratospheric. To estimate the SWV contribution of this RF, an estimation should be made of which part of the total emissions is stratospheric.

Due to the assumptions on the amount of emissions that take place in the stratosphere and the fact that the current implemented H_2O response surface already takes both stratospheric and tropospheric H_2O emissions into account. A model determining the impact of SWV due to direct emissions will not be implemented.

This will cause the total amount of SWV to be underestimated, as the SWV caused by direct emission will be quantified in the H_2O module and not in the SWV module of OAC. Therefore, possible saturation effects of the SWV will not be perfectly modelled. However, it is not foreseen that this will cause significant errors. Partly due to the emissions taking place in the lower part of the stratosphere, which already has a shorter lifetime than the upper part and the minor amount of flights that take place in the stratosphere.

3.3. H_2O Transport from the Troposphere Evaluation

Aviation-induced changes in stratospheric water vapour may, in principle, arise from enhanced transport of tropospheric water vapour across the cold-point tropopause due to global warming caused by aviation emissions. However, this pathway will not be explicitly represented in the OpenAirClim framework.

OpenAirClim is a reduced-form climate response model that does not resolve cold-point tropopause temperatures, stratospheric circulation, or dynamical transport processes. Therefore, an order-of-magnitude assessment is conducted to evaluate whether aviation-induced changes in tropospheric water vapour transport are sufficiently large to warrant explicit modelling. This assessment, presented in Appendix A, shows that the magnitude of this effect is negligible relative to natural variability and model uncertainty. In addition to that, the influence of aviation emissions on the water vapour transport into the stratosphere is a feedback effect of the emissions. Consequently, this pathway is excluded from further analysis in this thesis.

3.4. Hydrogen Leakages

There are two ways H_2 leakages cause SWV. One path is to obtain SWV via the oxidation of H_2 in the stratosphere, the other is due to the reaction of H_2 with OH, causing the OH concentration to decrease and therefore increasing the CH_4 concentration and with that also the SWV concentration due to CH_4 oxidation (Gunter, 2024; Warwick et al., 2022). These two paths are also shown in Figure 3.1. In Figure 3.1, E_{H_2} is the emission of H_2 in kg, $\Delta[H_2]$ is the change in H_2 concentration expressed in ppbv, Δm_{SWV} is the change in SWV mass expressed in kg, ΔRF_{SWV} is the change in RF caused by SWV expressed in Wm^{-2}, $\Delta\tau_{CH_4}$ is the change in lifetime of CH_4 in years, and $\Delta[CH_4]$ is the change in CH_4 concentration expressed in ppbv. The arrows, a through f, are used to explain the relations between the species.

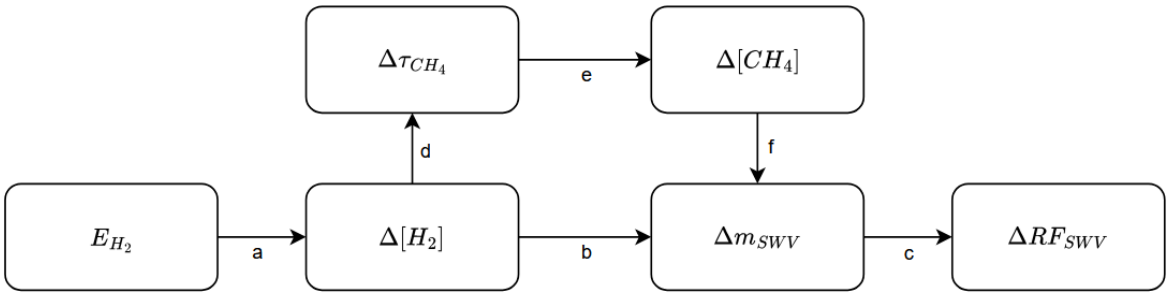

Figure 3.1: Overview of the influence of H_2 emissions on SWV mass and RF. The letters at the arrows relate to the processes described below.

a. Relation between E_{H_2} and $\Delta[H_2]$.
To relate an H_2 emission to a concentration change, the model of Bertagni et al. (2022) is used. This model relates an H_2 emission to an H_2 concentration change using the CH_4 background concentration and the OH background concentration. This model is also used by Gunter (2024) and is already implemented in OAC, using data from the Coupled Model Intercomparison Project (CMIP6).

b. Relation between $\Delta[H_2]$ and Δm_{SWV}.
For this relation, Warwick et al. (2022) developed a method. They state that the amount of SWV formed by a surface concentration increase of 1500 ppbv is approximately ($\pm$ 20%) equal to the amount of SWV formed due to methane oxidation between 1950 and 2000, which is described by Myhre et al. (2007). Warwick et al. (2022) also assume the relation between the surface concentration of H_2 and the amount of SWV is linear. Using the data of Myhre et al. (2007), which is also used to estimate SWV due to CH_4 oxidation (section 3.1), the mass of the formed SWV can be determined.

c. Relation between Δm_{SWV} and ΔRF_{SWV}.
When using the change in SWV perturbation mass in Equation 2.10 from Pletzer (2024) the total RF of SWV due to H_2 leakages can be determined. The procedure for this can be read in section 3.1.

d. Relation between $\Delta[H_2]$ and $\Delta\tau_{CH_4}$.
The H_2 surface concentration can be linked to a change in CH_4 lifetime using Figure 4C of Warwick et al. (2022) (stated as Figure 3.2 in this thesis). In Figure 3.2, a linear relation between the H_2 surface concentration and the CH_4 lifetime is displayed. The coloured dots relate to the data points for the experiments performed by Warwick et al. (2022), the black solid line is the fit through experiments in which only H_2 is changing. The black dashed line is the fit to the experiments in which CH_4 responds to changes in atmospheric H_2 (and OH). The relation shown by the dashed line can be used in OAC, to calculate the change in CH_4 lifetime due to changing H_2 concentrations.

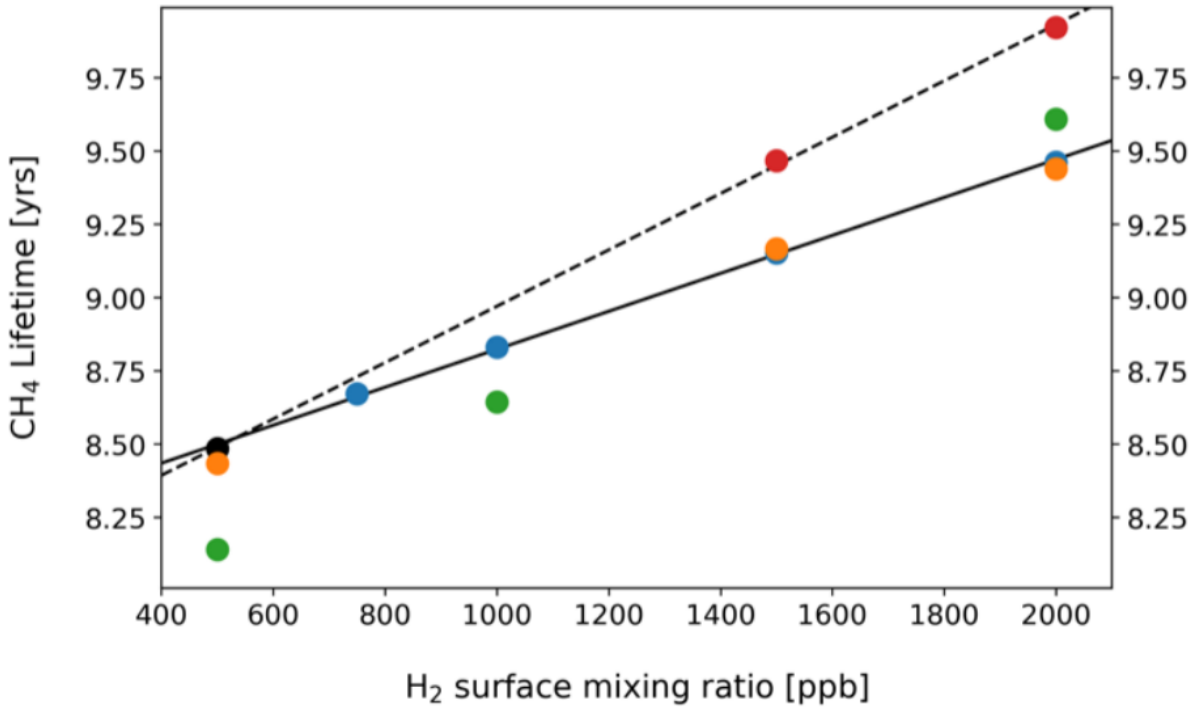

Figure 3.2: CH_4 lifetime plotted as a function of the H_2 surface mixing ratio. The coloured dots relate to specific experiments, see Warwick et al. (2022) for the exact description. The black solid line is the fit through experiments in which only H_2 is changing. The black dashed line is the fit through the experiments in which CH_4 responds to changing atmospheric H_2 (and OH). (Taken from Warwick et al. (2022)).

e. Relation between $\Delta\tau_{CH_4}$ and $\Delta[CH_4]$.
The change in lifetime of CH_4 can then be converted to a change in CH_4 concentration using the perturbation method of Grewe and Stenke (2008). This perturbation method was implemented in older versions of AirClim (Grewe & Stenke, 2008), but should be implemented in OAC for calculating CH_4 concentration changes due to the change in lifetime due to H_2 emissions.

f. Relation between $\Delta[CH_4]$ and Δm_{SWV}.
When a change in CH_4 concentration is obtained, the same method as for CH_4 oxidation described in section 3.1 can be applied to get to an SWV mass.

Including these six steps in OAC will give estimations for SWV formed due to H_2 leakages. However, in this thesis, this will not be included for two reasons. First, this thesis focuses on SWV formed due to aviation emissions. H_2 is not directly emitted by aviation, it is more of a secondary effect. When there are more aircraft flying on hydrogen in the future, hydrogen leakages will also occur on a larger scale causing H_2 emissions. Second, in OAC, there is already a machine learning model estimating the impact of H_2 emissions developed by Gunter (2024). In this model, also SWV effects are estimated, this is why there is no direct need to implement a second method, although this model could increase the confidence in the machine learning method from Gunter (2024).

4

Verification and Validation

To ensure reliability, the implementation of the SWV module in OAC is verified and validated. In section 4.1, the verification is performed. In this section, it will be checked if the methodology is properly implemented and no errors are made in the implementation. In section 4.2, the validation is performed, where cross-checks are made with literature-derived values.

4.1. Verification

In this verification section, it is checked if the model that is built, is correctly built and no errors are made during the implementation. This is done in the following steps. First, it will be checked if the fractional release factor (α) and the age-of-air (AoA) are correctly calculated in subsection 4.1.1. Second, the vertical distribution of SWV for three reference scenarios is determined and verified in subsection 4.1.2. Third, a method to check if correct mass quantities are calculated must be included as well, this is done in subsection 4.1.3. Last, the step to relate the SWV mass to an SWV radiative forcing is verified in subsection 4.1.4.

4.1.1. Fractional Release Factor and Age-of-Air

To verify if the fractional release factor (α) and the Age-of-Air are properly determined, the constructed α is compared with the α determined by Hegglin et al. (2014). The AoA is verified by comparison with other literature.

The constructed vertical profile of α is shown in Figure 4.1. The small spots visible in the lower tropical region are numerical artefacts associated with the troposphere at that altitude. Since the troposphere is not considered in the analysis, these artefacts do not affect the results. When comparing the constructed α with the α from Hegglin et al. (2014) (stated in Figure 4.2), the data clearly displays the same behaviour, only the α determined by Hegglin et al. (2014) is about 0.1 lower at the tropics and there is a mismatch at the values close to the south pole, where Figure 4.2 shows higher values, while in the reconstruction this effect is not visible.

Although, the values do not exactly match the constructed values closely resemble the data derived by Hegglin et al. (2014), the small mismatch is logical due to different input data. Also, the mismatch at the poles can be neglected as the volumes at these latitudes are much smaller than at the equator.

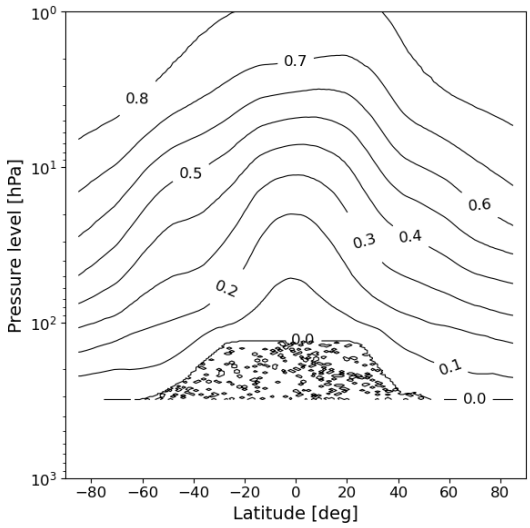

Figure 4.1: The constructed vertical profile of α using the newly developed OAC model.

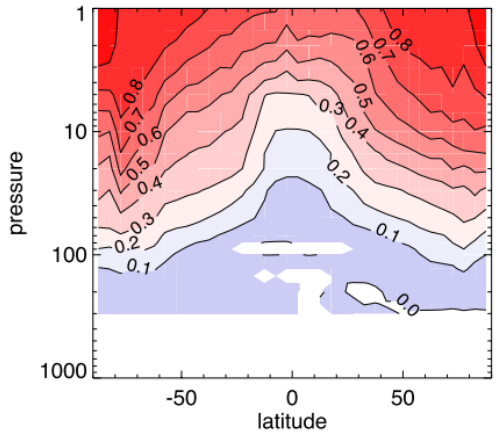

Figure 4.2: The spatial profile of α determined by Hegglin et al. (2014). (Figure taken from the supplement of Hegglin et al. (2014))

When looking at values for the AoA, the values are comparable with literature. Chipperfield et al. (2014), Garny et al. (2024), and Waugh and Hall (2002) all found a similar relation and similar latitude-altitude dependent AoA values. An extra check is performed to estimate the mass weighted average AoA of the stratosphere, this is calculated using the formula stated in Equation 4.1. Where AoA_{mw} is the mass-weighted AoA, AoA_i is the AoA of every grid cell i, m_i is the mass of every grid cell. This results in a mass weighted AoA of 1.4 years. Which corresponds to the value estimated by Garny et al. (2024).

$$AoA_{mw} = \frac{\sum_i (AoA_i \cdot m_i)}{\sum_i m_i} \tag{4.1}$$

4.1.2. Spatial SWV Distribution

To verify if the method to calculate the SWV mass increase due to an increase in global CH_4 concentration is implemented correctly, the values stated in Figure 2 of Myhre et al. (2007) are reproduced, as the method described by Myhre et al. (2007) is similar to the method used in OAC. This reproduction is done by running the model for the corresponding increase in methane. So for the periods of 1750-2000, 1950-2000, and 1979-2000, the increase in global methane concentration is 1047, 614, 212 ppbv, respectively (Meinshausen et al., 2020). The SWV distribution generated using OAC is plotted and compared with Figure 2 of Myhre et al. (2007). This can be seen in Figure 4.3, where the figure of Myhre et al. (2007) is plotted in black and the data resulting from the developed method is plotted with dashed green contours. It can be seen that the constructed lines closely resemble the black contours, especially in Figure 4.3a and Figure 4.3b, where the lines almost perfectly overlap. In Figure 4.3c, the constructed SWV concentration for a concentration of 0.4 ppmv is not shown. This is due to the method in OAC slightly underestimates the plots of Myhre et al. (2007) and therefore the 0.4 ppmv is not reached. The ppmv value in the upper stratosphere does come close, with values at 60 km altitude of 0.388 ppmv near the poles and values of 0.376ppmv at the tropics. These slight differences can be caused by the fact that Myhre et al. (2007) use different entry methane concentrations, or use a slightly different atmospheric composition than used in OAC, as well as the different model that is used by Myhre et al. (2007). Although there are slight differences, which are normal when not using the exact same method, it can be concluded that the method for determining the spatial distribution of SWV is correctly implemented.

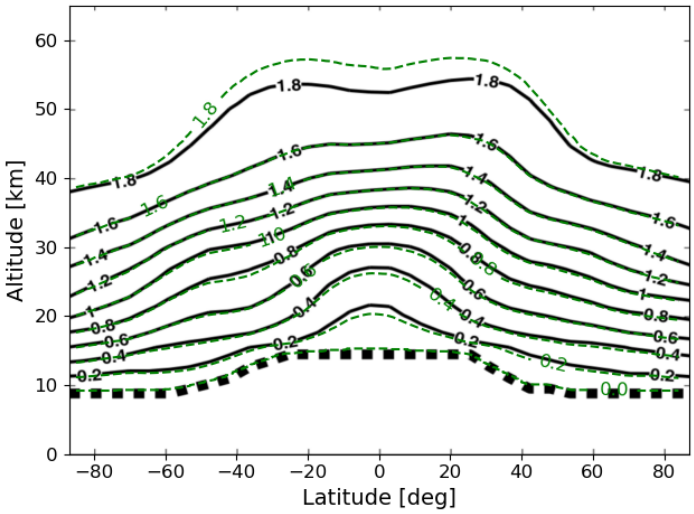

(a) SWV concentration in ppbv due to a methane concentration change equal to the methane concentration change from 1750-2000

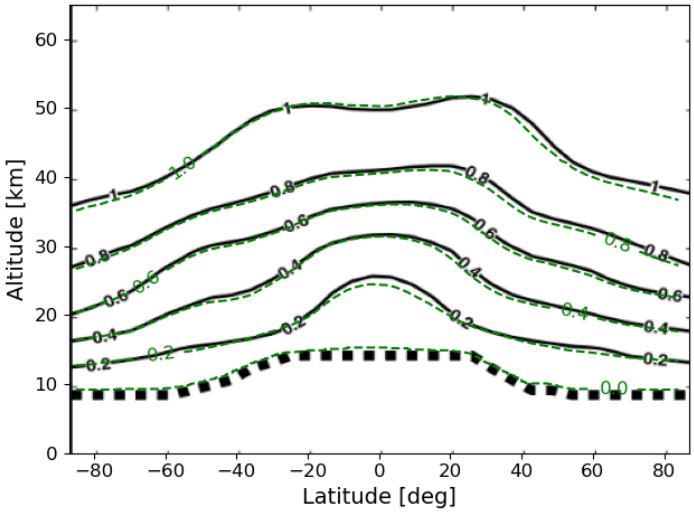

(b) SWV concentration in ppbv due to a methane concentration change equal to the methane concentration change from 1950-2000

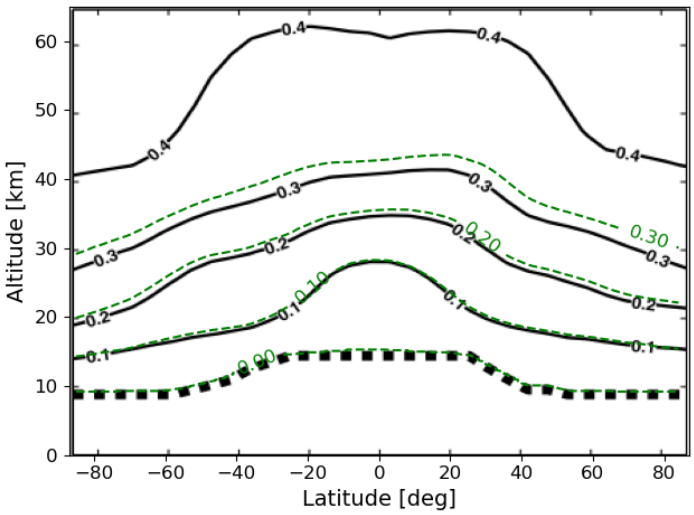

(c) SWV concentration in ppbv due to a methane concentration change equal to the methane concentration change from 1979-2000

Figure 4.3: In this figures the SWV concentration is plotted caused by certain global CH_4 changes. The black lines are taken from Myhre et al. (2007) figure 2a, 2b and 2c. The newly generated data using OAC is plotted on top of the data from Myhre et al. (2007) with a dashed green line.

4.1.3. SWV Mass

The applied method has already been verified, and the concentration changes calculated are correct. However, to ensure consistency, the absolute mass flux of CH_4 into the stratosphere should also be verified.

A consistency check was performed for the period 1979-2000, as the stratospheric CH_4 loss for this interval has been determined by Kirschke et al. (2013).

To estimate the increase in SWV mass over this period, the first-order mass balance equation stated in Equation 4.2 is used. In this equation, m_{SWV} is the total mass of SWV in the stratosphere in Tg, P_{SWV} is the production rate of SWV (Tg yr^{-1}), and τ_{SWV} is the mean lifetime of SWV in years, approximately equal to the age of air (AoA) in the stratosphere as there is hardly any chemical loss (Fueglistaler et al., 2013; le Texier et al., 1988).

$$\frac{dm_{SWV}}{dt} = P_{SWV} - \frac{m_{SWV}}{\tau_{SWV}} \tag{4.2}$$

Under steady-state conditions the mass does not change ($\frac{dm_{SWV}}{dt} = 0$), Equation 4.2 simplifies to Equation 4.3. This steady state assumption is valid as the production rates are assumed constant during the whole decade (Kirschke et al., 2013) and SWV has an average lifetime of approximately 1.4 years (Garny et al., 2024), which is much smaller than a decade.

$$P_{SWV} = \frac{m_{SWV}}{\tau_{SWV}} \quad \text{or equivalently} \quad m_{SWV} = P_{SWV} \cdot \tau_{SWV} \tag{4.3}$$

The change in SWV mass (Δm_{SWV}) can then be expressed as the difference between the 1990s and 1980s as displayed in Equation 4.4, where $P_{SWV,90}$ and $P_{SWV,80}$ represent the SWV production rates for the 1990s and 1980s, respectively.

$$\Delta m = (P_{SWV,90} - P_{SWV,80}) \cdot \tau_{SWV} \tag{4.4}$$

The SWV production can be derived from the CH_4 loss rate, as it is assumed that each CH_4 molecule produces two SWV molecules through oxidation (Frank et al., 2018; le Texier et al., 1988). The estimated annual stratospheric CH_4 loss is approximately 46 Tg yr^{-1} during the 1980s and 67 Tg yr^{-1} during the 1990s (Kirschke et al., 2013). Using the molar masses of the gases, 1 Tg of CH_4 corresponds to 2.25 Tg of SWV. Therefore, $P_{SWV,90}$ equals 150.75 Tg(SWV) yr^{-1} and $P_{SWV,80}$ equals 103.5 Tg(SWV) yr^{-1}.

The lifetime τ_{SWV} is determined using the mass-weighted average age of air. When computing a mass-weighted average of the age of air for the stratosphere, a mean AoA of 1.4 years is found (see subsection 4.1.1 and Garny et al. (2024)). This is physically consistent, as most of the stratospheric mass resides in the lower stratosphere, where the AoA is shortest. Since there is negligible chemical loss of SWV in the stratosphere (Fueglistaler et al., 2013; le Texier et al., 1988), the residence time of CH_4-derived SWV is approximated by the local mean age of air, equalling 1.4 years (Hall & Plumb, 1994; Hall & Waugh, 2000; Holzer et al., 2012).

Using the lifetime of 1.4 years, Equation 4.4 can be substituted and the change in SWV mass becomes:

$$\Delta m_{SWV} = (150.75 - 103.5) \times 1.4 = 66.3 \text{ Tg(SWV)}$$

From the OAC model, a value of 59 Tg of SWV is obtained. This result is in the same order of magnitude as the SWV mass estimated using the mass method. Considering the uncertainties in the CH_4 loss estimates reported by Kirschke et al. (2013), the steady state assumption, the simplification of AoA and the uncertainty in the yield. It can be concluded that the model calculations are done correctly and are properly implemented.

4.1.4. Conversion of SWV Mass to a RF

To verify if the method to determine the RF due to SWV is correctly modelled, the data is compared to Fig 7.17 of Pletzer (2024). When the fit proposed by Pletzer (2024) is plotted in Figure 4.4 (blue line) alongside some randomly chosen modelled SWV perturbation masses in OAC (blue dots), it can be seen that the modelled masses are exactly on the curve. The only exception occurs for the values that should have a negative RF according to the fit of Pletzer (2024). In these cases, the RF is set to zero as described in section 3.1, since the RF value becoming negative is caused by a mismatch of the fit rather than reality.

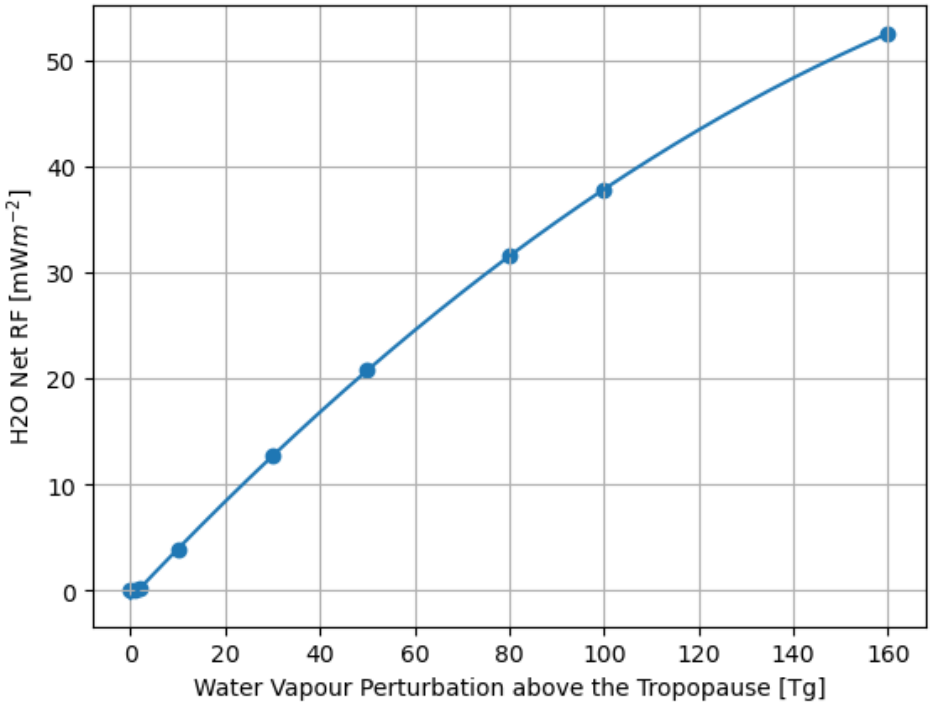

Figure 4.4: The polynomial fit from Pletzer (2024) (blue line) with some test SWV perturbation masses and their corresponding RF value (blue dots).

4.2. Validation

Validation assesses whether the implemented model represents physical reality. In contrast to verification, which focuses on internal correctness of the model, validation evaluates model results against independent literature-derived estimates of SWV RF due to CH_4 oxidation. The objective of the SWV module within OAC is to provide physically consistent estimates of the climate impact of SWV perturbations with the correct order of magnitude, rather than to reproduce any climate-chemistry model exactly.

In this section, the RF calculated by OAC is compared to established results from the literature, primarily Myhre et al. (2007). In addition, known model limitations identified from previous studies are discussed to contextualise the validation results.

4.2.1. Comparison with Myhre et al. (2007)

Myhre et al. (2007) quantified the radiative forcing due to stratospheric water vapour produced from methane oxidation for several historical methane perturbation periods. They reported that the SWV RF amounts to approximately 15-20% of the direct methane radiative forcing, with absolute SWV RF values of approximately 83, 50, and 16 mW m^{-2} for the periods 1750-2000, 1950-2000, and 1979-2000, respectively.

To validate the OAC SWV module, these scenarios were reproduced using the methane concentration changes reported by Meinshausen et al. (2020). The resulting SWV mass perturbations were converted

to radiative forcing using the relationship derived by Pletzer (2024).

For the period 1750-2000, no RF value is computed by OAC, as the associated SWV mass perturbation exceeds the validity range of the radiative forcing parameterisation used in this study. The fit of Pletzer (2024) is explicitly limited to SWV mass increases below 160 Tg, whereas the 1750-2000 methane perturbation produces substantially larger SWV increases, of the order of 240 Tg.

For the remaining periods, the comparison between Myhre et al. (2007) and OAC is shown in Table 4.1. For the 1950-2000 period, the RF estimated by OAC (49 mW m^{-2}) agrees closely with the value reported by Myhre et al. (2007) (50 mW m^{-2}). For the 1979-2000 period, OAC yields an RF of 20 mW m^{-2}, compared to 16 mW m^{-2} reported by Myhre et al. (2007). Although this corresponds to a relative difference of approximately 25%, the values remain of the same order of magnitude and well within the uncertainty associated with differing modelling approaches.

Overall, this comparison demonstrates that the OAC SWV module produces radiative forcing estimates that are consistent with established literature values, supporting its validity for climate impact assessments.

Table 4.1: Comparison of radiative forcing due to stratospheric water vapour from methane oxidation between Myhre et al. (2007) and OpenAirClim.

Period	RF Myhre et al. (2007) [mW m^{-2}]	RF OAC [mW m^{-2}]
1750-2000	83	-
1950-2000	50	49
1979-2000	16	20

4.3. Discussion

This section discusses the limitations and findings of the verification and validation. It also interprets the implications of these limitations.

One limitation for validating the model is the lack of suitable literature. This is due to most literature focusing on SWV production and not solely on the part related to CH_4 oxidation. The publications that focus specifically on SWV formed by CH_4 oxidation mostly take NO_x emissions as their input. This however, could not be done in OAC as the module that relates NO_x emissions to CH_4 concentration changes is not validated yet. In this way, no valid conclusions could be drawn from these end-to-end validation procedures. Next to this, there are also no publications found that look into the transient response of SWV to a change in methane concentration. The literature does state radiative forcing at a certain time, which is not directly steady state, as the methane changes of the previous year are not fully oxidized to SWV. However, no conclusions could be drawn, as no data is provided about how much of the CH_4 has already oxidised at that time.

Several limitations of the current SWV modelling approach should be acknowledged when interpreting the validation results. First, multiple studies have shown that SWV concentrations are influenced not only by methane oxidation, but also by changes in tropopause temperatures and stratospheric transport (e.g.Fueglistaler et al. (2013) and Revell et al. (2016)). Warming of the cold-point tropopause due to global warming can therefore have a larger impact on SWV concentrations than aviation-induced changes in CH_4 concentrations alone, an effect that is not represented in the present SWV module.

Second, the yield of water vapour from CH_4 oxidation is assumed to be constant and equal to two water molecules per CH_4 molecule. While this is a common approximation, Frank et al. (2018) demonstrated that the effective yield can deviate from this value depending on altitude and chemical pathways. This introduces additional uncertainty into the absolute magnitude of the simulated SWV perturbations. The magnitude of this uncertainty can be read in chapter 5.

Third, the radiative forcing parameterisation applied in this study is non-linear and has a limited range of validity, as discussed in section 3.1. As a consequence, SWV perturbations larger than 160 Tg cannot be reliably translated into RF values using the current formulation. This limitation restricts the applicability of the model to perturbations comparable to present-day or near-future scenarios. Furthermore, Pletzer (2024) only considers increases in SWV concentrations, while aviation emissions tend to

decrease the amount of SWV due to the decreased methane concentration. The saturation behaviour captured by the non-linear relationship derived by Pletzer (2024) reflects a progressive humidifying of the stratosphere. When this relationship is used for decreases in water vapour, the implied saturation would instead correspond to an extreme depletion of water vapour, approaching undersaturated or nearly dry conditions. However, such a regime is not physically realistic. In the real atmosphere, the stratosphere cannot fully dry out because multiple transport pathways continuously supply water vapour from the troposphere. Consequently, the saturation effects in the relation, when decreasing the amount of water vapour, do not represent a physically meaningful limitation, but rather an artefact of extrapolating the original non-linear fit beyond the conditions for which it was derived.

Finally, the assumption is made that the fractional release factor will stay constant over time. This is valid as long as the atmospheric conditions stay comparable with the atmospheric composition used to determine this fractional release factor, which is the 1991-1999 atmosphere. Future projections show that this might significantly differ, as methane concentrations could grow or shrink with 50% (Meinshausen et al., 2020), atmospheric temperature is possibly rising with more than $2^{\circ}C$(IPCC, 2013), which could significantly influence stratospheric residence time and oxidation speed.

Despite these limitations, the verification and validation steps provide confidence that the implemented SWV module captures the dominant physical mechanisms relevant for scenario-based climate impact assessments.

5

Sensitivity and Uncertainty Analysis

This chapter presents a sensitivity analysis of the parameters governing the production of SWV by methane oxidation and its associated radiative forcing. This analysis aims to identify which parameters dominate the resulting RF perturbations. Next, an uncertainty analysis is presented to identify the magnitudes of the uncertainties for different scenarios.

The parameters considered in this study are explained in section 5.1 and are summarized in Table 5.1. Each parameter is varied independently within the range indicated in the table, while all remaining parameters are held constant. The resulting sensitivities are stated in section 5.2. The uncertainty analysis is explained and performed in section 5.3 followed by the conclusion of this chapter in section 5.4.

5.1. Sensitivity Parameters

The parameters included in the sensitivity analysis, together with their standard values and assigned uncertainty ranges, are summarized in Table 5.1, where the parameter, its unit, the standard value for the parameter, and the uncertainty range can be found. In the following paragraphs, each parameter and its scientific basis are discussed in more detail.

Reference Tropospheric CH_4 concentration ($CH_{4,\mathrm{ref}}$)

The first parameter is the reference tropospheric methane concentration, $CH_{4,\mathrm{ref}}$, which is used to construct the α distribution. This value represents the tropospheric mean methane concentration (and therefore the stratospheric entry concentration) corresponding to the observational period of Myhre et al. (2007). The standard value of 1.772 ppmv is taken from the estimate for the year 1999 reported by the National Oceanic and Atmospheric Administration (NOAA).[1] Hegglin et al. (2014) states that, at a different interval (2005-2006) of the same data, the uncertainty range is ± 0.014 ppmv based on interannual variability and measurement uncertainty. As it is the same dataset, this uncertainty range is used as well for the $CH_{4,\mathrm{ref}}$ value used.

Reference Stratospheric CH_4 Distribution

Uncertainty in the reference vertical methane distribution affects the shape of the α profile and therefore the derived SWV production. The reference stratospheric methane distribution used is the profile measured with the Halogen Occultation Experiment (HALOE), as is used in the paper of Myhre et al. (2007). Park et al. (1996) estimate that HALOE methane measurements are accurate within approximately 15%.

This 15% error margin is included at the top of the distribution. The layer high up in the stratosphere, where a concentration of methane of 0.2 ppmv is measured, is varied with $\pm$ 15%. This error margin is then linearly decreased to the tropopause, where the error on the measurement is 0. This is done to

[1] https://gml.noaa.gov/webdata/ccgg/trends/ch4/ch4_annmean_gl.txt, accessed 05-12-2025

assure compatibility with the $CH_{4,ref}$ value, which is the tropopause value and is varied separately. The value should be compatible, as otherwise a total increase of methane levels close to the tropopause would cause higher values in the stratosphere than at the tropopause, causing negative values for α, which have no scientific meaning. The decision to implement the error margin in this way is made, as this sensitivity is done to find the effects of parameters on the SWV output, rather than diving into the uncertainty of HALOE satellite measurements, as that is out of scope for this thesis.

Age of Air

The age of air (AoA) is computed using the empirical relation introduced by Hegglin et al. (2014) (Equation 3.3), which links AoA to the α distribution. Since no formal error bars for this empirical fit are provided, the uncertainty is estimated from the spread of observations in Figure S5 of Hegglin et al. (2014). A range of ± 0.3 years is adopted, which encloses nearly all observational points and ensures that the resulting AoA remains strictly positive.

Yield of SWV per Oxidised CH_4 (y_{SWV})

The SWV yield from CH_4 oxidation is taken as $y_{\mathrm{SWV}} = 2$ mol mol^{-1} (le Texier et al., 1988). However, Frank et al. (2018) demonstrate a clear altitude dependence, with values ranging from 1.4 to 2.2 depending on altitude. This range is adopted here, to account for chemical variability and uncertainty of the yield.

Radiative Sensitivity

The RF per Tg SWV (named radiative sensitivity) is based on the polynomial fit presented by Pletzer (2024) in his Figure 7.17 and in Equation 2.10. Because this fit is empirical and no uncertainty is provided by Pletzer (2024), an uncertainty of $\pm 10\%$ is applied. This uncertainty is determined by looking at the data from Figure 7.17 of Pletzer (2024), with an uncertainty of 10%, all data points fit within the range.

Table 5.1: Parameters used in the sensitivity analysis, including their unit, standard value, and uncertainty range.

Parameter	Unit	Standard value	Range	Source
$CH_{4,\mathrm{ref}}$	ppmv	1.772	± 0.014	Hegglin et al. (2014), NOAA
Reference stratospheric CH_4 distribution	ppmv	See Fig. 1 of Myhre et al. (2007)	$\pm 15\%$	Myhre et al. (2007); Park et al. (1996)
AoA	yr	See Equation 3.3	± 0.3	Hegglin et al. (2014)
y_{SWV}	mol mol^{-1}	2.0	1.4–2.2	Frank et al. (2018)
Radiative sensitivity	W m^{-2} Tg^{-1}(H_2O)	See Equation 2.10	$\pm 10\%$	Pletzer (2024)

5.2. Local Sensitivity Analysis

A local (one-at-a-time) sensitivity analysis is performed using the parameter ranges in Table 5.1. For each parameter, the model is run while perturbing only that parameter and keeping all others fixed. All simulations take a step increase of 100 ppbv in methane as input. This 100 ppbv methane change is chosen as it is a representative scenario for aviation emissions (see chapter 6). The sensitivity results are displayed in Figure 5.1 for the steady state output and in Figure 5.2, the output two years after the methane concentration change is displayed. In these figures, the effect of the parameter perturbation is expressed as a relative percentage change in RF.

For the steady state, analysis shows that the largest sensitivity arises from the SWV yield, y_{SWV}, which exhibits an approximately linear effect on the RF, a 10% increase in the yield produces a 10% increase in RF, and likewise for decreases.

The second most influential parameter is the stratospheric CH_4 distribution (HALOE profile). A 15%

decrease in the CH_4 distribution causes the SWV RF to increase by 12%, while a 15% increase of the CH_4 distribution causes the SWV RF to decrease by 12%.

The radiative sensitivity parameter also shows linear behaviour, a 10% increase of the parameter causes the outcome to increase by 10% and vice versa.

$CH_{4,\mathrm{ref}}$ has an impact of $\pm 3\%$ in RF, which is larger than the uncertainty assigned to this parameter of $\pm$ 0.8%.

The AoA perturbation has the weakest effect (-1.2%, +0.2%), consistent with the fact that AoA primarily influences adjustment time scales rather than the steady-state magnitude of the SWV forcing.

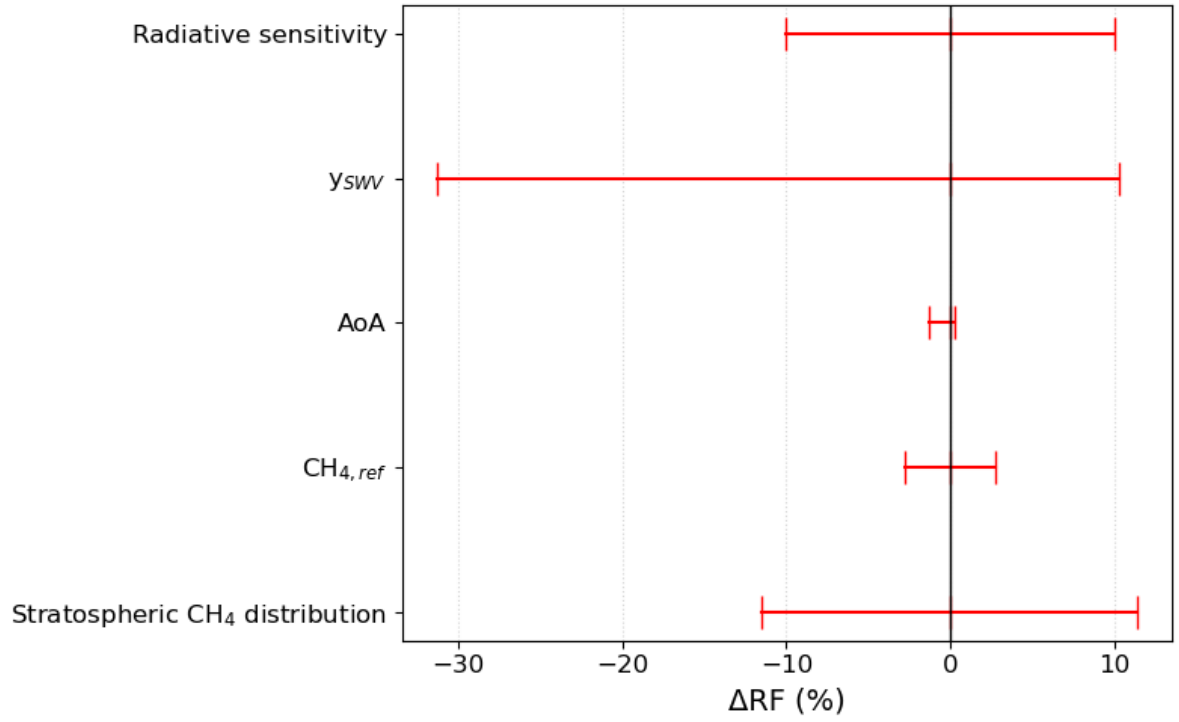

Figure 5.1: Results for the local sensitivity analysis for a 100 ppbv methane concentration change. The shown results are for the steady state outcome.

In addition to the steady-state response, the transient response is also analysed. The sensitivity of the model output to the parameters under transient conditions is illustrated in Figure 5.2. The transient sensitivities are evaluated two years after the emission perturbation.

As shown in Figure 5.2, the AoA exerts a substantially larger influence on the output in the transient regime than in the steady state, with a contribution of approximately 32% compared to about 3% in steady-state conditions. In contrast, the sensitivity associated with the stratospheric CH_4 distribution is noticeably lower in the transient case compared to the steady state case. This reduced sensitivity arises from the definition of the stratospheric CH_4 uncertainty, which is largest in the upper stratosphere. Two years after the emission, these higher stratospheric layers have not yet been affected by the CH_4 concentration perturbation, as vertical transport processes operate on longer timescales. Consequently, uncertainties in these regions have a limited impact on the transient response at this point in time. The other three parameters, radiative sensitivity, yield of SWV, and the reference methane concentration, do not show remarkable differences compared to the steady state sensitivity.

Overall, the sensitivity analysis indicates that uncertainties in the chemical yield of SWV primarily affect the magnitude of long-term SWV forcing estimates, while dynamical parameters such as age of air are more critical for short-term projections. This distinction provides a clear framework for interpreting the subsequent uncertainty analysis and for identifying priorities in future efforts to reduce uncertainty in

methane-induced SWV radiative forcing estimates.

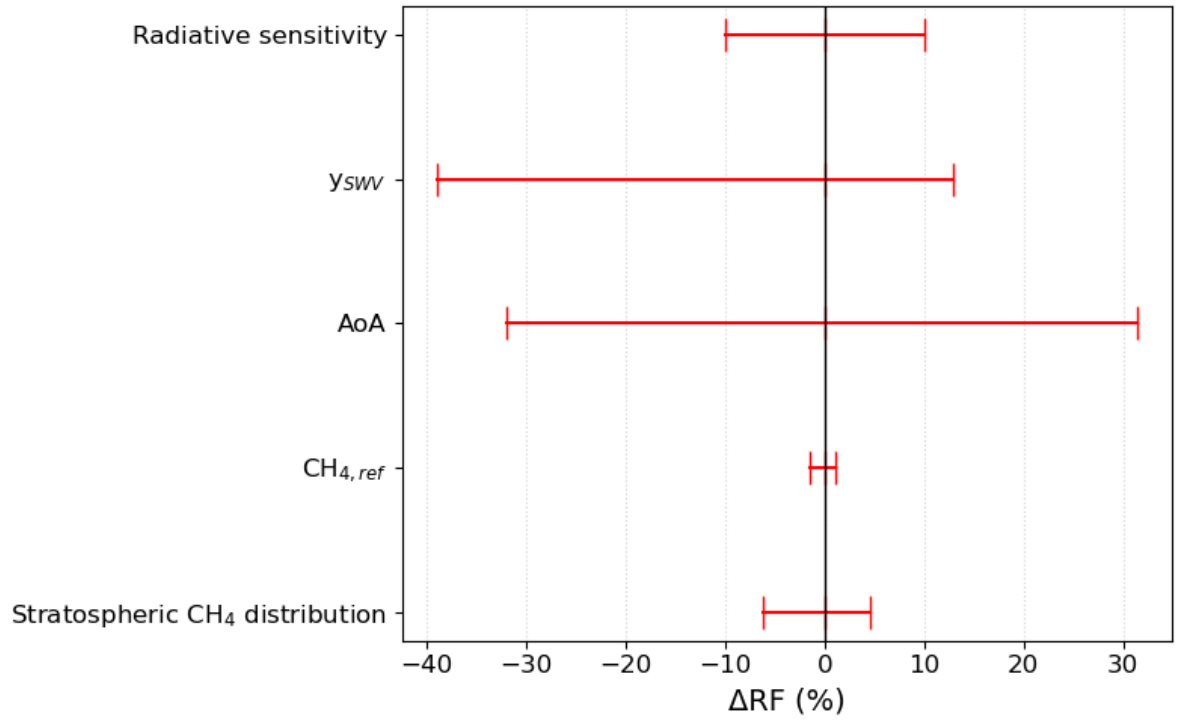

Figure 5.2: Results for the local sensitivity analysis for a 100 ppbv methane concentration change. The output is obtained two years after the change in methane concentration.

5.3. Uncertainty Analysis

In this section, the uncertainty of the model is determined. This will be done by examining the RF in the year 2100 due to the scenarios defined in subsection 6.1.1 and testing whether these scenarios are significantly different from each other when the uncertainty of the input parameters is taken into account. In subsection 5.3.1, the methodology of the Monte Carlo analysis is explained and how it relates to the uncertainty of the model. In subsection 5.3.2, the outcomes of the Monte Carlo analysis are stated. In subsection 5.3.3, the scenarios are statistically analysed to see if they are significantly different from each other.

5.3.1. Monte Carlo Framework and Paired Sampling

To assess the robustness of the scenario results under parameter uncertainty, a Monte Carlo analysis was conducted for all four scenarios defined in subsection 6.1.1. The analysis builds on the preceding sensitivity study, which identified the most influential input parameters affecting radiative forcing. Monte Carlo simulations were implemented using a paired sampling approach for all uncertain parameters common to the scenarios (for the parameters see Table 5.1). In this approach, each Monte Carlo iteration uses a single random realization of the uncertain parameter set, which is applied consistently to all scenarios. Thus, for iteration i, the same sampled values of CH_4 concentration, stratospheric distribution, AoA, SWV yield, and radiative sensitivity are used when computing the radiative forcing for every scenario. As a consequence, the radiative forcing results obtained for different scenarios within the same iteration are directly comparable and differ only due to scenario-specific assumptions rather than random parameter variation. The scenario outputs are therefore statistically paired on an iteration-by-iteration basis. This paired design reduces Monte Carlo sampling noise and allows differences between scenarios to be attributed solely to scenario assumptions, thereby increasing the statistical power of the subsequent scenario comparison.

A total of 500 Monte Carlo simulations is performed, resulting in paired estimates of radiative forcing for each scenario. The number of runs of 500 is determined by running the model 100 times and then

estimating the coefficient of variation (c_v). An additional run is done and the c_v is determined, this is repeated until the c_v stabilizes (less than 1% difference in the last 5 runs). If the c_v is stable, the Monte Carlo analysis is stopped and the number of runs is determined, in this case 500.

When the data from the Monte Carlo simulation is obtained, it is analysed and the mean and standard deviation are determined, giving insight into the uncertainty of the model. The distributions of the Monte Carlo simulation are also tested for significant differences between the scenarios to see if they are significantly different. The Wilcoxon signed-rank test is used for this test because it does not assume normality of the data and is suitable for paired data.

5.3.2. Distribution of Radiative Forcing Outcomes

The Monte Carlo simulations yield distributions of radiative forcing values for the scenarios rather than single deterministic values. The probability density functions (pdf) of these distributions are shown in Figure 5.3. From Figure 5.3, it can be seen that the mean values for the distributions are -21, -31, -8.3, and -7.8 mW m^{-2} for the scenarios BAU, CurTec, FP2050, and FP2050cont (for the definition of the scenarios, see subsection 6.1.1). These scenarios have a standard deviation of 3.0, 4.1, 1.3, and 1.3 mW m^{-2}, respectively. This standard deviation is approximately 15% of the mean for all four scenarios. It can be observed that all pdfs have an approximately normal distribution and that the pdfs for the FP2050 and FP2050cont scenarios are nearly identical and have a smaller standard deviation than those for the BAU and CurTec scenarios.

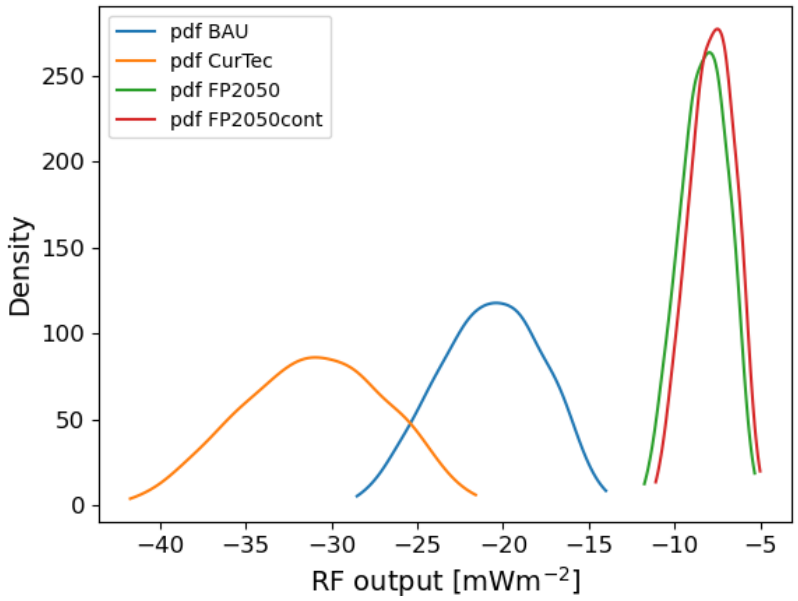

Figure 5.3: The probability density functions for the scenarios BAU (blue), CurTec (yellow), FP2050 (green), and FP2050cont (red) determined by the Monte Carlo analysis.

5.3.3. Statistical Assessment of Scenario Differences

From Figure 5.3 it appears that in some cases the RF outcome for certain scenarios might be equal to the value from another scenario. However, as the values are paired, this might not be the case. To test this, the difference in radiative forcing was computed for each simulation run (i), calculated using Equation 5.1, where an example is shown for the BAU and CurTec scenarios. The subscript i denotes the Monte Carlo iteration, such that both radiative forcing values are computed using the same realization of the uncertain input parameters.

$$\Delta RF_{BAU-CurTec_i} = RF_{BAU_i} - RF_{CurTec_i} \tag{5.1}$$

Calculating this difference for all combinations of scenarios, six distributions are obtained. These six distributions are displayed in Figure 5.4 and Figure 5.5. In Figure 5.4, the differences between the BAU scenario and the Curtec, FP2050, FP2050cont scenarios are displayed in blue, yellow, and green, respectively. The differences between the CurTec and the FP2050 and FP2050cont scenarios are shown in red and purple, respectively. The difference between the FP2050 and FP2050cont scenario is shown in a separate figure, Figure 5.5, because it exhibits a peak several orders of magnitude larger than the other distributions.

From Figure 5.4 and Figure 5.5, it can be observed that the differences relating to FP2050 and FP2050cont are very similar. This is logical as the pdf functions for these two scenarios are also very similar.‘ It can also be noticed that the peak of the FP2050-FP2050cont distribution is much higher and the spread is smaller than the other distributions. For exact numbers, see Table 5.2, where the mean, standard deviation, and p-value of the statistical test are stated for all six scenarios. Furthermore, it can be seen that none of the paired difference distributions include zero mWm^{-2} in their range, indicating that scenario outcomes remain distinct across all Monte Carlo realizations.

To absolutely assure that the observed differences between both scenarios are statistically distinguishable, a Wilcoxon signed-rank test was applied to the paired Monte Carlo results. This test evaluates whether the median of the paired differences in radiative forcing is equal to zero, making it well-suited for the present analysis.

The test strongly rejects the null hypothesis of zero mean difference as the p-value is in the order of 10^{-83} for all six scenarios. This indicates a statistically significant difference in radiative forcing between each combination of two scenarios.

Table 5.2: Mean, standard deviation, and p-value of the Wilcoxon signed-rank test for all six pairwise differences between the four scenarios.

Scenario	BAU–CurTec	BAU–FP2050	BAU–FP2050cont	CurTec–FP2050	CurTec–FP2050cont	FP2050–FP2050cont
Mean [mW m^{-2}]	-10.4	-12.5	-13.0	-22.9	-23.4	-0.5
Standard deviation [mW m^{-2}]	1.2	1.7	1.7	2.8	2.9	0.07
p-value	10^{-83}	10^{-83}	10^{-83}	10^{-83}	10^{-83}	10^{-83}

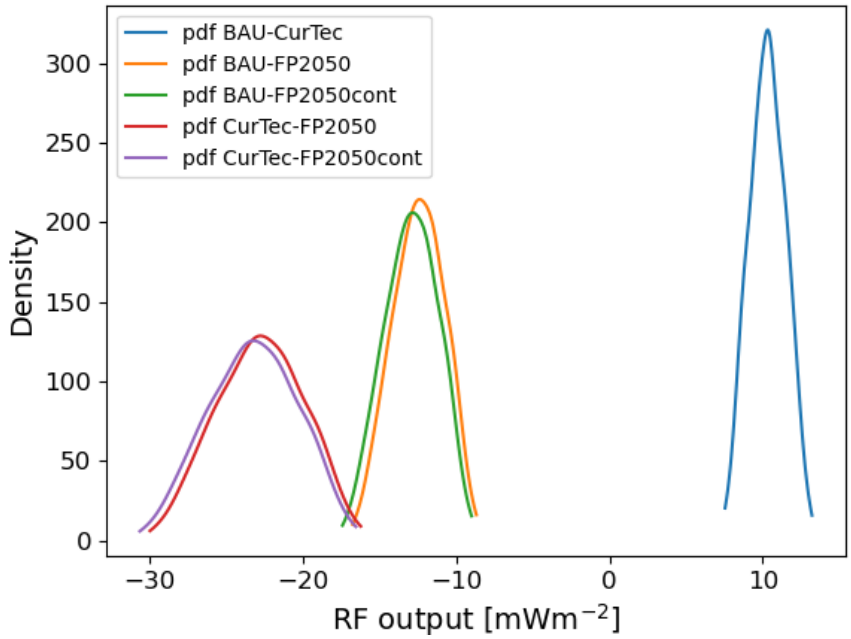

Figure 5.4: The pdf of the difference between the BAU scenario and the Curtec, FP2050, FP2050cont scenario are displayed in blue, yellow, and green, respectively. The difference between the CurTec and the FP2050 and FP2050cont scenarios are shown in red and purple, respectively. The difference between the FP2050 and FP2050cont scenario is shown in a separate figure, Figure 5.5. For the values of the mean and the standard deviation, see Table 5.2.

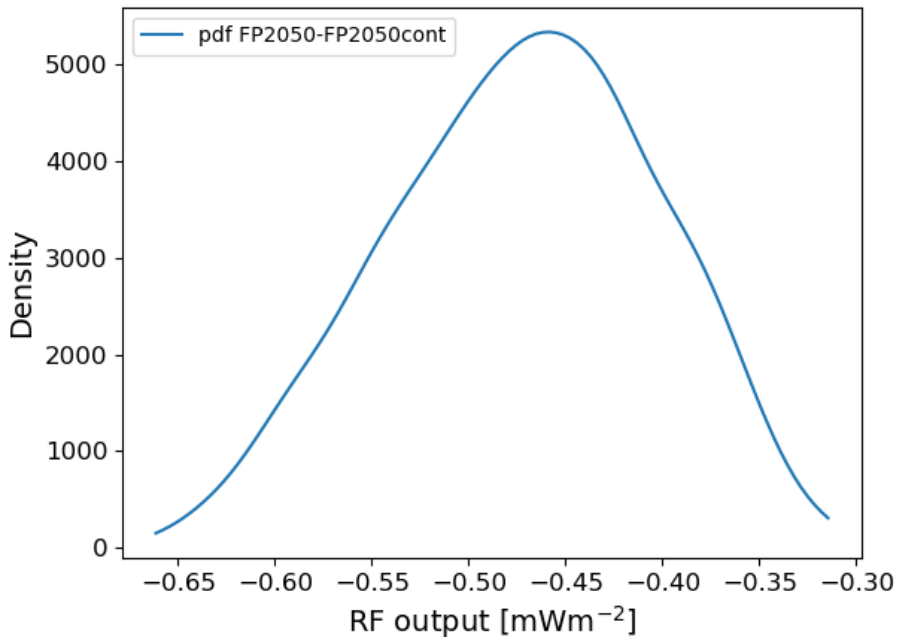

Figure 5.5: The pdf of the difference between the FP2050 and FP2050cont output for every Monte Carlo run. For the values of the mean and the standard deviation, see Table 5.2.

5.4. Conclusion

This chapter investigated the sensitivity of SWV radiative forcing to key model parameters and assessed how uncertainties in these parameters propagate into uncertainty in the model output. The combined sensitivity and uncertainty analyses provide important insight into both the robustness and limitations of the implemented SWV module within the OpenAirClim framework.

The sensitivity analysis demonstrates that the model response is dominated by a limited number of parameters, being the reference stratospheric methane concentration and stratospheric distribution defining the fractional release factor, the chemical yield of SWV from methane oxidation, and the parameterizations governing age-of-air and radiative forcing. The strong influence of the methane reference concentration highlights the importance of accurately representing stratospheric conditions, as small relative changes in this parameter translate into larger changes in radiative forcing.

A distinction emerges between steady-state and transient behaviour. While the chemical yield and methane-related parameters dominate the steady-state response, the AoA exerts a substantially larger influence under transient conditions. This reflects the role of stratospheric transport timescales in shaping the temporal evolution of SWV following changes in methane concentrations. As a result, uncertainties related to the age-of-air are especially relevant for short-term (less than 5 years) climate responses, whereas chemical and radiative parameters primarily control long-term outcomes.

The uncertainty analysis shows that absolute estimates of SWV radiative forcing exhibit a standard deviation of approximately 15% of the mean value across the considered scenarios. While this level of uncertainty limits the precision of absolute forcing estimates, it is consistent with uncertainties typically associated with simplified climate response models (Lee et al., 2021). Importantly, the paired Monte Carlo framework demonstrates that relative differences between scenarios remain stable across the uncertainty range. The statistical analysis confirms that scenario differences are robust and statistically significant, indicating that parameter uncertainty does not obscure the relative ranking of aviation scenarios.

These findings imply that the model is well-suited for comparative assessments. The robustness of relative scenario differences supports the use of the OAC SWV module for evaluating mitigation strategies and future aviation pathways. This is particularly relevant for assessments where relative changes, rather than absolute magnitudes, drive policy-relevant insights.

6

Scenario Analysis

In this chapter, some future scenarios will be analysed and the effect of SWV in these scenarios will be monitored. The scenarios considered are taken from Grewe et al. (2021), where different scenarios for plausible future developments of aviation are described. The scenarios considered are: Current technology (CurTec), Business as usual (BAU), Flight Path 2050 (FP2050), and Flight Path 2050 continuously implemented (FP2050cont). These scenarios are described in detail in section 6.1 together with the background scenarios that are taken into account and the outputs that will be computed. In section 6.2, the outcome of the model for the different scenarios is stated. A discussion of the results and the conclusions drawn from them are presented in section 6.3.

6.1. Scenario Analysis Setup

In this section, all scenarios that are used as inputs and all output parameters are described. The section starts with subsection 6.1.1, where the four scenarios used for this scenario analysis are explained. Next, in subsection 6.1.2, the different background scenarios are stated and explained. In the last section, subsection 6.1.3, the outputs that are considered in this scenario analysis are described.

6.1.1. Scenarios

The scenarios that are used for this analysis are derived from Grewe et al. (2021). In this thesis, five scenarios are proposed to describe how aviation and its emissions will evolve until the year 2100. Grewe et al. (2021) report the CO_2 and NO_x emissions on a yearly basis. The model developed takes tropospheric methane concentration as an input, so the NO_x emissions are related to a CH_4 concentration change using OAC. Note that this module in OAC is not yet validated, but the results are only to give insight into how future SWV RF might develop for different emission scenarios. The given changes in methane concentrations can be found in Figure 6.1. In Figure 6.1, the change in methane concentration is plotted versus time in the future for the four scenarios. BAU is plotted in blue, CurTec in red, FP2050 in grey, and FP2050cont in purple. The scenarios are the same from 1940 to 2020. Therefore, the data from 1940 to 2010 has been omitted. It can be seen from Figure 6.1 that the scenarios start to deviate after 2020. The changes in methane concentration vary from -90 ppbv to -380 ppbv depending on the scenario. Below, the four different scenarios used will be explained.

Current Technology (CurTec)

CurTec represents a “no-action” baseline scenario in which aviation continues operating with 2012-level technology and no additional political or technological measures are implemented. Aircraft fuel efficiency, engine performance, NO_x emissions, and operational characteristics remain frozen at their 2012 state.

Business as Usual (BAU)

The BAU scenario assumes that aviation evolves according to expected improvements in fuel efficiency and technology, but without specific interventions driven by climate policies. It incorporates the

historically observed trend of incremental efficiency improvements, better operations, and natural fleet renewal, but does not include ambitious emissions targets or offset schemes. It depicts how the sector would develop under typical industry behaviour.

Flightpath 2050 (FP2050)

This scenario implements the Advisory Council for Aviation Research and Innovation in Europe (ACARE) Flightpath 2050 targets (*Flightpath 2050*, 2011), which require 75% reduction in CO_2 emissions per passenger-km, 90% reduction in NO_x emissions, and 65% reduction in perceived noise, all relative to a typical aircraft in the year 2000. FP2050 assumes that the advanced technologies needed to reach these goals are developed first and only introduced into the market around 2050, meaning the benefits appear relatively late. It results in strong emissions reductions, but with a noticeable overshoot in climate impact around mid-century.

Flightpath 2050, Continuous Introduction (FP2050cont)

FP2050cont uses the same ACARE performance targets as FP2050 but assumes a smooth, continuous, and earlier introduction of advanced technologies, rather than a delayed deployment. New efficient aircraft begin entering the market sooner, and improvements diffuse into the fleet more gradually over time. This leads to earlier climate benefits and a more consistent reduction trend. Among all scenarios, FP2050cont provides the pathway most compatible with achieving aviation's share of the Paris Agreement goals.

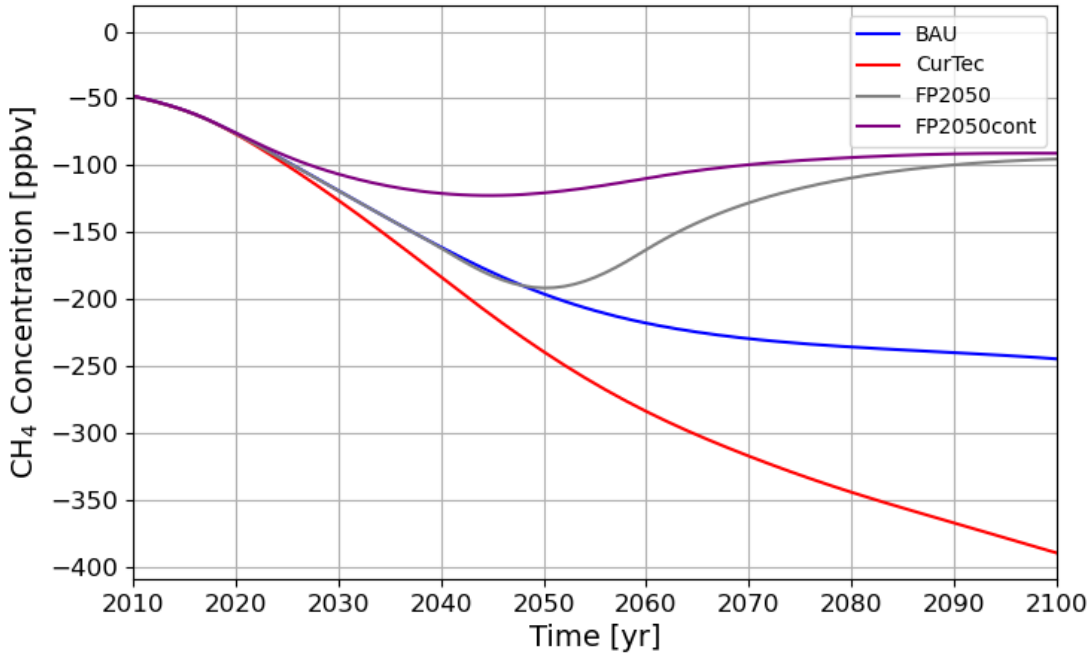

Figure 6.1: The input tropospheric CH_4 change for the four different scenarios. Based on the NO_x emission data from Grewe et al. (2021) and related to CH_4 concentration changes using OAC. The background scenario used in SSP2-4.5.

6.1.2. Backgrounds

Next to the scenarios, also the background is of influence for future predictions of SWV forcing due to aviation emissions. As the scenarios model the aviation emissions, the backgrounds represent the influence of all other changes in the atmospheric composition.

In this thesis, the background will be modelled using the shared socio-economic pathway (SSP) scenarios explained by Meinshausen et al. (2020). Five pathways are defined for future development, sustainability, middle of the road, regional rivalry, inequality and fossil-fuel development, numbered

one to five, respectively. These pathways are linked to future predictions for the RF in the year 2100 with respect to pre-industrial levels. THe RF value for 2100 forms the suffix of the SSP scenario name. So, SSP1.1-9 means that pathway one (sustainability) is used, with a total RF in 2100 of 1.9 W m^{-2}. The SSP scenarios used in this thesis are SSP1-1.9, SSP2-4.5, SSP3-7.0, and SSP4-6.0. These background scenarios are chosen as they are part of the main SSP scenarios according to Meinshausen et al. (2020) and assure a representative scenario for all possible future scenarios.

The differences in future global methane background concentrations can be seen in Figure 6.2, where the evolution of methane concentration for the different SSP scenarios is displayed over time. In this figure, it can be seen that, in general, the SSP scenarios with a higher RF also have higher methane concentrations and that the range of the methane concentrations in 2100 varies widely from 1000 ppbv in SSP1-1.9 to 3300 ppbv in SSP3-7.0.

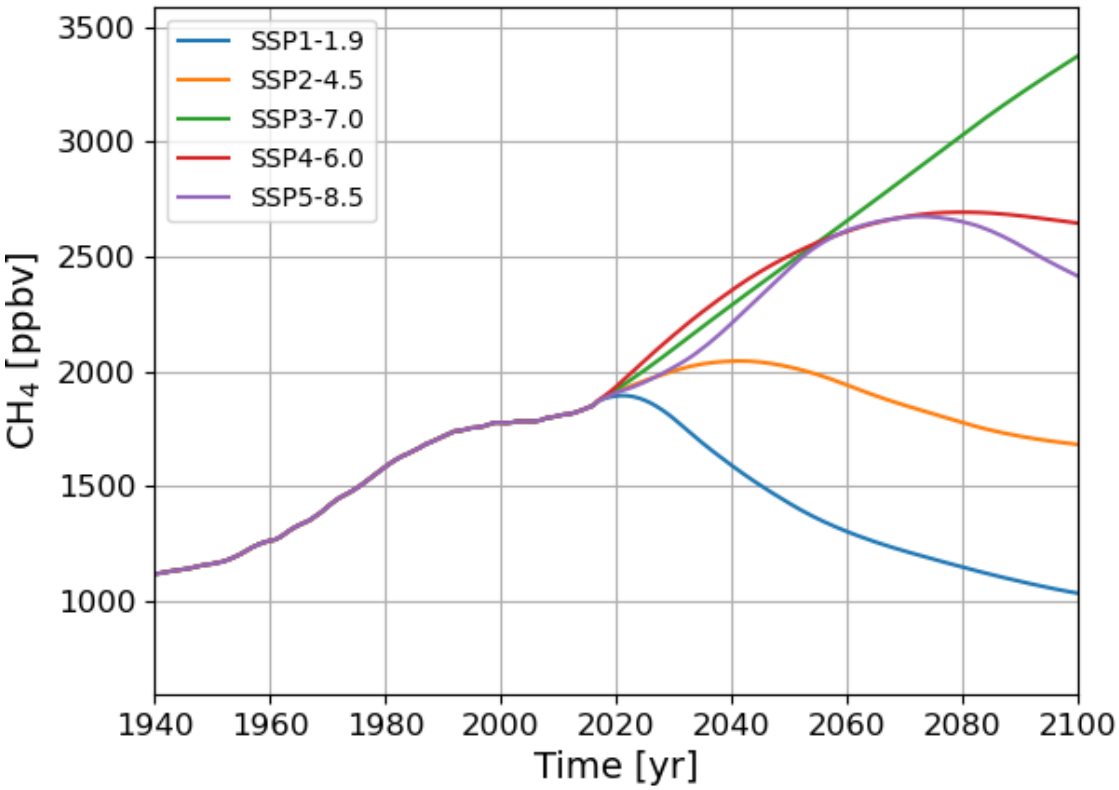

Figure 6.2: The global methane background concentration for different SSP scenarios as determined by Meinshausen et al. (2020)
. SSP1-1.9 is displayed in blue, SSP2-4.5 is displayed in yellow, SSP3-7.0 is displayed in green, SSP4-6.0 is displayed in red, and SSP5-8.5 is displayed in purple.

6.1.3. Outputs

The outputs that are considered in this scenario analysis are the change in RF due to SWV (RF_{SWV}) and the ratio of the RF due to SWV divided by the RF of CH_4 (also referred to as ratio). These two outputs are selected because they directly quantify the magnitude of the SWV-induced radiative response and its relative importance compared to the primary radiative forcing from methane, thereby allowing for a clear, interpretable comparison across scenarios and background conditions. Other metrics like the GWP and ATR can be found in Appendix B as they are produced as part of the modelling workflow. They are not included in the main text as the patterns they exhibit are similar to those of RF_{SWV}.

6.2. Scenario Results

The results of the different inputs are presented here. In subsection 6.2.1, the RF_{SWV} for the different scenarios and backgrounds is displayed. In subsection 6.2.2, the effect of the scenarios and the background on the ratio between RF_{SWV} and RF_{CH_4} is stated. Other climate metrics (dT, GWP20 and ATR20) and more detailed plots can be found in the Appendix B.

6.2.1. Stratospheric Water Vapour Radiative Forcing (RF_{SWV})

The RF impact of SWV varies depending on the scenario and the background. For the different scenarios, a simulation is run with the background of SSP2-4.5. The resulting RF_{SWV} is displayed in Figure 6.3. In this figure, the data from before 2010 is omitted as it is the same for all scenarios. It exhibits a smooth increase from the 1940s to the value in 2010. Until 2023, all scenarios appear to be the same. After 2023, they start to differ from each other. For the FP2050 (grey line) and FP2050cont (purple line) scenarios, it can be seen that the RF forcing experiences a minimum around the years 2052 and 2048, respectively, while the BAU (blue line) and CurTec (red line) scenarios are solely decreasing. It should be noted that this plot with RF values is very similar to the plot of the global tropospheric methane concentrations that are used as input (Figure 6.1). There are some small mismatches, like the year at which the minimum value is achieved, which is slightly lagged for the RF response, which is logical as there is some time required for the methane concentration change to oxidise to SWV. Looking at the actual values, the FP 2050 and FP2050cont scenario both end up with a forcing in 2100 of -9 mW m^{-2}, while the BAU scenario has a RF at 2100 of -23 mW m^{-2} and the CurTec scenario of -35 mW m^{-2}. So the scenarios where emissions are reduced the most have the least effect on the SWV radiative forcing.

When looking at the background scenarios, it is beneficial to look at the relative impact of a changing background. In Figure 6.4, the relative impact compared to the reference, SSP2-4.5, is displayed. Here, all background scenarios have the same linestyle such that they can be distinguished, the colours refer to the scenario with the same convention as for Figure 6.3. The most prominent feature in the figure is the horizontal dashed line at a value of one. This is the reference SSP scenario (SSP2-4.5) and therefore defined to be constant at one. Furthermore, it can be seen that all the solid lines (SSP1-1.9) are below the reference scenario and all follow a similar trajectory. From this, it can be concluded that the SSP scenario does influence the outcome, but its relative influence is not really dependent on the different future scenarios. As can be seen from the two other background scenarios as well. It must also be noted that the spread of the dash-dotted (SSP4-6.0) and especially the dotted (SSP3-7.0) lines is larger than the spread of the solid line. This corresponds with the magnitude of the methane background concentration. This implies that when the methane background concentration is higher, it will have relatively more influence on the SWV RF for each future scenario. More detailed figures for all scenarios and background scenarios are stated in Appendix B section B.1.

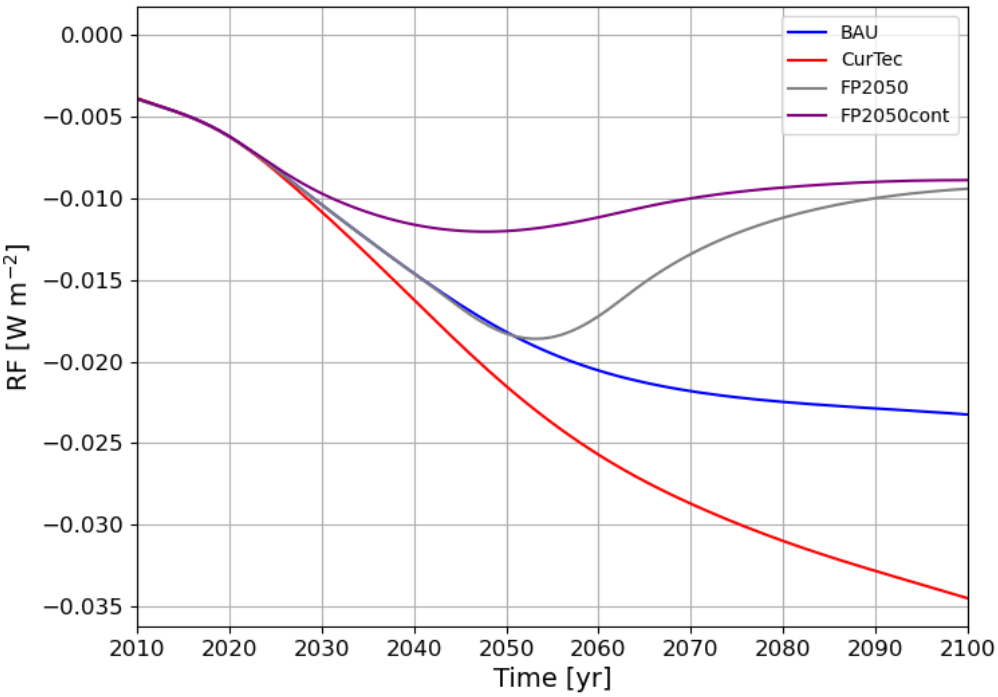

Figure 6.3: The RF due to SWV over the period 2010-2100 for the four different scenarios (BAU, CurTec, FP2050, and FP2050cont shown in blue, red, grey, and purple, respectively) using SSP2-4.5 as background.

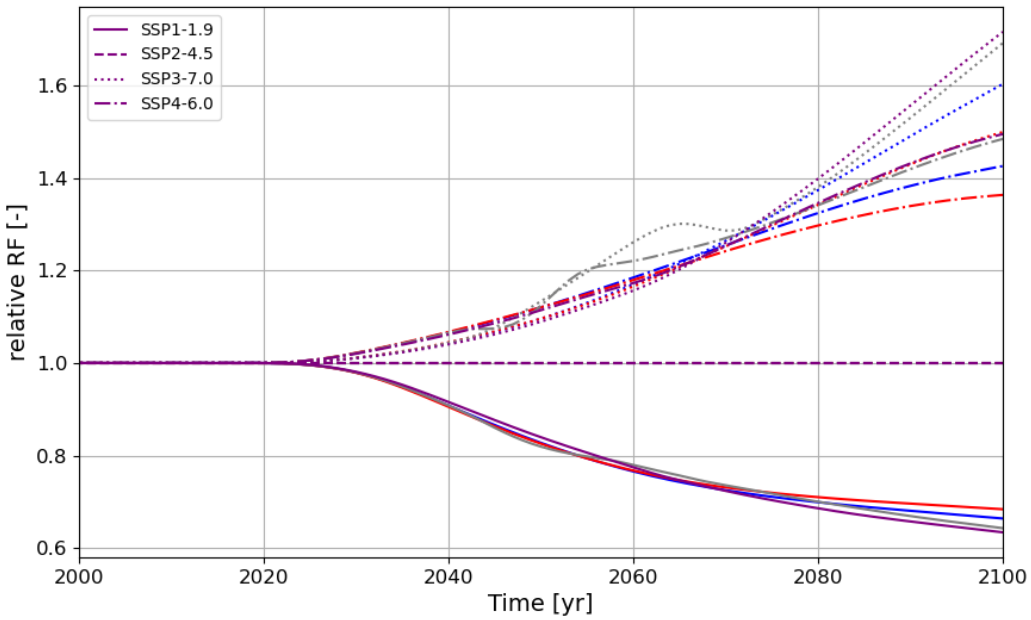

Figure 6.4: Relative impact of different background scenarios for the different future scenarios. The solid lines correspond to SSP1-1.9, dashed lines to SSP2-4.5, dotted lines to SSP3-7.0, and dash-dotted lines to SSP4-6.0. Colours refer to scenarios the same way as in Figure 6.3.

6.2.2. Ratio of RF_{SWV} over RF_{CH_4}

Another output that is considered is the ratio of RF_{SWV} over RF_{CH_4} referred to as ratio. This metric is worth looking into as it is widely used in publications to determine the SWV impact (Lee et al., 2021; Myhre et al., 2013) and gives insight into the relative importance of SWV compared to other climate forcers. In Figure 6.5, the ratio is plotted for the four scenarios for a set background equal to SSP2-4.5. It can be seen that the ratio varies from 0.18 to 0.24 over time, depending on the scenario. It appears that the ratio is not constant over time (as shown in Figure 6.5). While in literature this value is taken as constant (Lee et al., 2021; Myhre et al., 2007).

When looking at the influence of the background, stated in Figure 6.6, it can be seen that the background also influences the ratio. The colours and linestyles have the same configuration as in Figure 6.4. The pattern for the scenarios is also highly similar to that of Figure 6.4. It is important to note the magnitude, as for certain SSP3-7.0 scenarios, the relative ratio increases to almost 1.5, leading to a ratio of 0.3.

Furthermore, the ratio is estimated by Myhre et al. (2007) to be a constant of 15-20%, a value that is also used in the IPCC reports (IPCC, 2013). From the Figures 6.5 and 6.6, it becomes clear that there is a transient response in the ratio and that it is not constant. When the ratio is instead calculated under steady-state conditions, it is observed that the values converge to a constant value (19-22%) close to the value estimated by Myhre et al. (2007). This is displayed in Figure 6.7, where five different constant CH_4 concentration perturbations (-59, -119, -178, -238, and -257 ppbv) are modelled for a fixed background methane concentration in OAC.

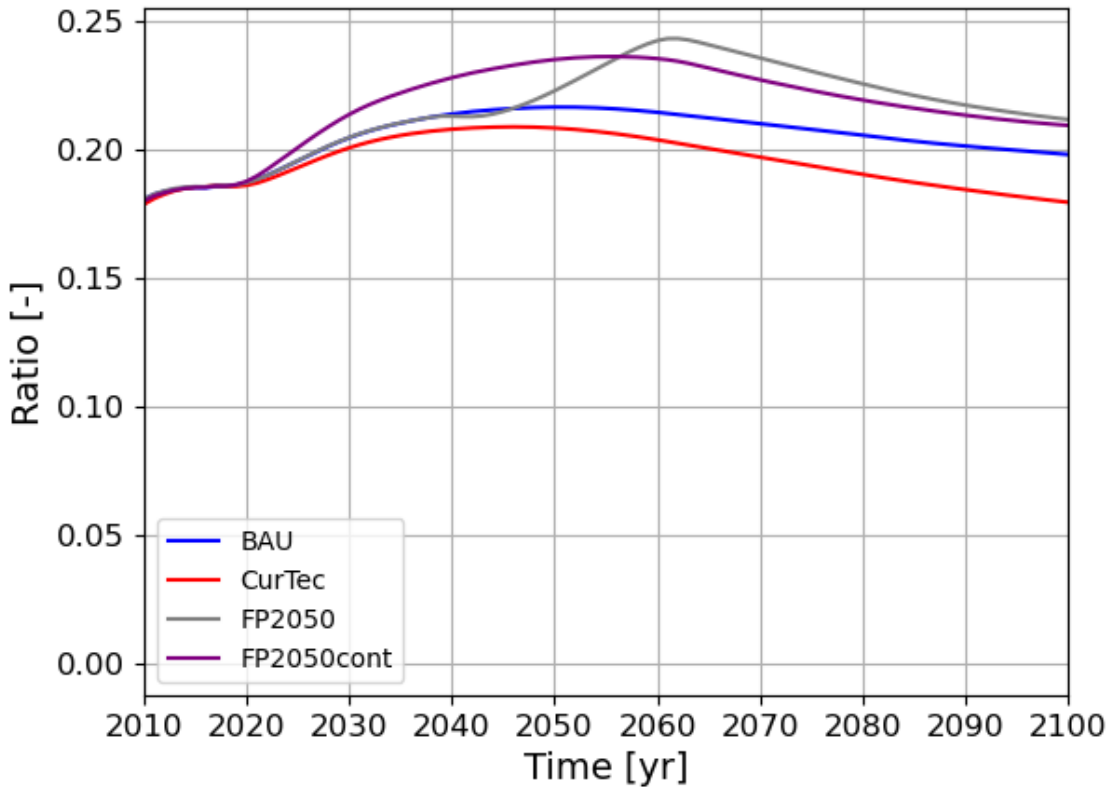

Figure 6.5: Ratio for the four different scenarios modelled with SSP2-4.5 as background scenario. Colours refer to scenarios the same way as in Figure 6.3.

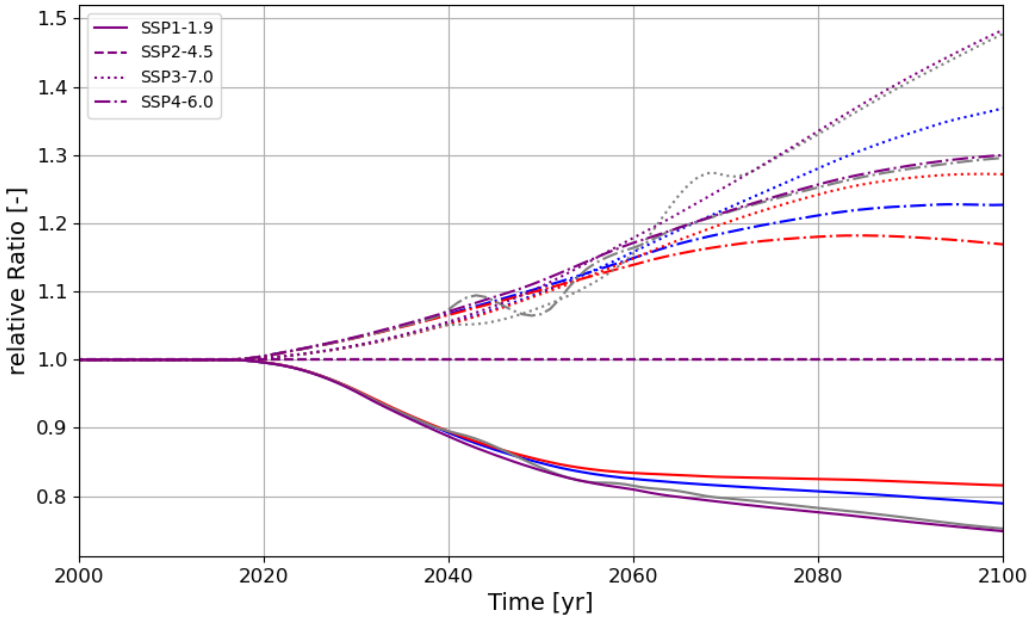

Figure 6.6: The relative impact of the background on the ratio. The same linestyle corresponds to the same background scenario. Colours refer to scenarios the same way as in Figure 6.3..

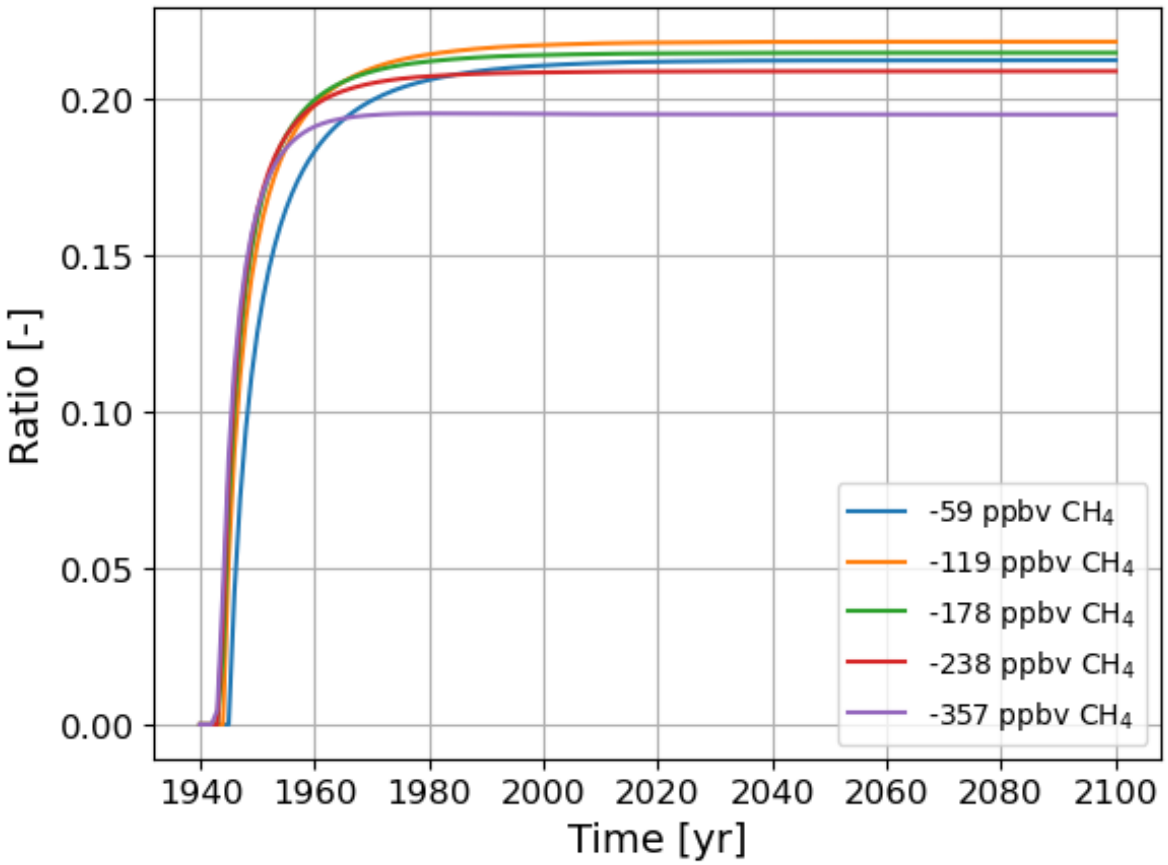

Figure 6.7: The ratio between SWV RF and CH_4 RF plotted for five different steady state CH_4 and SWV levels. The CH_4 steady state input concentrations are -59, -119, -178, -238, and -257 ppbv. Please note that the steady state ratio decreases for increasing change in CH_4 concentration, except for the value of -59, for which the ratio is a little lower.

6.3. Discussion and Conclusion

This chapter analysed the future evolution of SWV RF induced by aviation-related methane changes under a range of aviation emission scenarios and background scenarios. By combining aviation scenarios from Grewe et al. (2021) with SSP-based background methane concentrations (Meinshausen et al., 2020), the analysis provides insight into both the absolute magnitude of SWV radiative forcing and its relative importance compared to methane radiative forcing.

The results show that future aviation developments have a distinct effect on SWV radiative forcing. Scenarios with strong emission reductions, such as FP2050 and FP2050cont, lead to substantially lower SWV radiative forcing reductions by the end of the century compared to BAU and CurTec. In particular, the CurTec scenario results in the largest reduction of SWV forcing, reflecting the continued growth of aviation NO_x emissions. The FP2050cont scenario consistently exhibits the earliest and smoothest reduction in SWV forcing, highlighting the importance of early and gradual technology introduction rather than delayed implementation.

A clear correspondence is observed between the temporal evolution of SWV radiative forcing and the prescribed tropospheric methane concentration changes. The small time lag between methane concentration changes and the SWV radiative response is physically consistent and reflects the time required for the methane to oxidize and form stratospheric water vapour.

The SSP background scenarios also influence the magnitude of SWV radiative forcing. While the relative differences between aviation scenarios remain similar across backgrounds, higher background methane concentrations amplify the relative impact of SWV forcing. This effect becomes particularly pronounced in high-forcing pathways such as SSP3-7.0, where both the absolute forcing and the spread

between scenarios increase. These findings indicate that the climatic context in which aviation operates can significantly modulate its non-CO_2 impacts, even if aviation emissions themselves follow the same trajectory.

An important outcome of this analysis is the behaviour of the ratio between SWV radiative forcing and methane radiative forcing. Contrary to the commonly applied assumption of a constant ratio of approximately 15–20%, the results show that this ratio varies over time and across scenarios. Transient effects associated with changing emissions and evolving background methane concentrations lead to ratio values that can exceed the traditionally assumed range, particularly under high-methane background scenarios. Only under idealised, steady-state conditions does the ratio converge to a near-constant value consistent with earlier estimates. This demonstrates that applying a fixed ratio in future scenario assessments may oversimplify the climate response and underestimate the dynamic nature of SWV forcing.

Overall, this scenario analysis demonstrates that both aviation mitigation strategies and broader socio-economic developments play a crucial role in determining the future climate impact of aviation-induced SWV. Early and continuous technological improvements substantially reduce SWV forcing reduction, while high background methane concentrations can enhance its relative importance. The results underline the need for dynamic treatment of SWV effects in future climate impact assessments of aviation, rather than relying on static scaling relationships. Although the NO_x module in OpenAirClim is not yet fully validated, the findings provide valuable, qualitative insight into how aviation's climate effects may evolve under different future scenarios.

7

Conclusion

This thesis investigated how the climate impact of aviation-induced stratospheric water vapour (SWV) can be represented within a simplified climate response model. The primary objective was to develop, implement, and evaluate a physically grounded yet computationally efficient method to quantify SWV-related radiative forcing using the OpenAirClim (OAC) framework.

A comprehensive literature review identified four potential pathways through which aviation can influence SWV: methane (CH_4) oxidation, direct emission of water vapour above the tropopause, changes in troposphere-stratosphere exchange driven by aviation-induced warming, and hydrogen leakages. Of these pathways, CH_4 oxidation was identified as the dominant and most robust mechanism suitable for implementation within OAC. The other pathways were shown to be either of secondary importance, highly uncertain, or out of scope of the thesis and are therefore not implemented in OAC.

A new SWV module based on CH_4 oxidation was developed using established parametrisations linking methane loss to water vapour production in the stratosphere. The approach combines fractional release factors derived from Halogen Occultation Experiment (HALOE) observations, age-of-air estimations, and a mass-based conversion of SWV perturbations to radiative forcing using an empirical relationship. This method integrates well with the existing framework in OAC and preserves computational efficiency.

Verification and validation demonstrate that the implemented SWV module reproduces key features reported in the literature. The spatial distribution of SWV changes closely matches results from Myhre et al. (2007), and the magnitude of the resulting radiative forcing lies within reported uncertainty ranges. Mass-balance checks further confirm the internal consistency of the approach. These results indicate that the simplified representation captures the essential physical behaviour of aviation-induced SWV changes despite the absence of explicit climate chemistry modelling.

The sensitivity and uncertainty analysis identifies the dominant sources of uncertainty governing the simulated SWV radiative forcing and clarifies how these uncertainties propagate through the model. The results show that the model response is controlled by a limited number of physically meaningful parameters. While absolute estimates of SWV radiative forcing exhibit a one-standard-deviation uncertainty of approximately 15% of the mean, the relative differences between aviation scenarios remain robust across the explored uncertainty range. This demonstrates that parameter uncertainty does not compromise the comparative assessment of aviation scenarios, even though it constrains the precision of absolute forcing values.

These findings justify the use of the implemented SWV module for scenario-based comparisons rather than for precise quantification of absolute climate impacts. The robustness of relative scenario differences supports the application of OpenAirClim in policy-relevant assessments, where comparative insights into mitigation strategies are more important than exact forcing magnitudes.

The scenario analysis demonstrates that future aviation pathways lead to substantially different trajectories of stratospheric water vapour radiative forcing. Scenarios characterised by strong and early emission reductions, such as Flight Path 2050 and its continuous implementation, result in markedly

smaller reductions in SWV forcing compared to Business-as-Usual and Current Technology scenarios. These differences reflect the strong coupling between aviation-induced methane changes and the resulting SWV response. In addition, higher background methane concentrations amplify the absolute SWV forcing. This highlights that the broader climatic context in which aviation operates can significantly influence the importance of non-CO_2 effects.

From the scenario analysis, it also became clear that the ratio between SWV radiative forcing and methane radiative forcing is not constant over time or across scenarios. Transient effects and evolving background conditions lead to substantial deviations from commonly assumed fixed ratios. This demonstrates that static scaling approaches may oversimplify aviation's climate impact and supports the need for dynamic representations of SWV effects in future climate impact assessments of aviation.

This modelling approach with reduced complexity also imposes limitations that should be considered when interpreting the results. Several potentially relevant pathways were intentionally excluded from the implementation. Direct stratospheric water vapour emissions are already represented in OAC without a strict separation between tropospheric and stratospheric sources, which was considered of minor importance for the present analysis. Changes in troposphere–stratosphere exchange were shown to be small relative to CH_4 driven SWV changes, though they may become more relevant under future flight altitude distributions or alternative propulsion concepts. Hydrogen-related effects were excluded due to the availability of a machine learning module within OAC. Furthermore, the SWV representation relies on fixed fractional release factors and age-of-air distributions derived from historical observations, implicitly assuming a stationary stratospheric circulation. As climate change may alter stratospheric transport timescales (and may already have done so since the observational data originate from the 1990s), long-term projections should be interpreted as indicative rather than predictive. In addition, the conversion from SWV mass perturbations to radiative forcing is based on an empirical relationship that is valid within the perturbation range relevant for aviation but may introduce large uncertainties if extrapolated beyond this range.

Despite these limitations, the results are consistent with published estimates and provide valuable insight into the relative importance of SWV compared to other aviation climate effects. The developed module extends the applicability of OpenAirClim for rapid scenario assessments and enables consistent comparison of SWV effects with other aviation climate forcers. While it does not replace detailed climate chemistry modelling, the approach offers a tool for policy analysis and aircraft technology assessment, where computational efficiency is essential.

Future work could focus on updating the fractional release factors to better account for changes in stratospheric circulation and stratospheric OH concentrations, as well as incorporating more recent estimates of the water vapour yield per oxidised CH_4 molecule, including altitude-dependent values such as those proposed by Frank et al. (2018). In addition, future work could focus on refining the method used to relate SWV perturbations to radiative forcing, as the current approach is primarily valid for perturbations smaller than 160 Tg and may lose accuracy when larger deviations from the reference state occur. Also, a hydrogen-related module could be implemented in OAC based on the methodology description in this thesis, to validate the machine learning module currently present in OAC. Furthermore, once the relationship between aviation NO_x emissions and methane lifetime has been validated within OAC, end-to-end tests of the full modelling chain could be performed to further increase confidence in the SWV module.

Overall, this thesis shows that simplified climate response models can meaningfully capture aviation-induced stratospheric water vapour effects. While the approach is not intended to replace comprehensive chemistry–climate models, it provides valuable insight into the relative importance and temporal evolution of SWV forcing across future aviation scenarios. As such, the developed framework contributes to more complete and transparent assessments of aviation's non-CO_2 climate impacts and supports informed decision-making in the context of long-term aviation mitigation strategies.

References

Austin, J., Wilson, J., Li, F., & Vömel, H. (2007). Evolution of water vapor concentrations and stratospheric age of air in coupled chemistry-climate model simulations. *Journal of the Atmospheric Sciences*, *64*, 905–921. https://doi.org/10.1175/JAS3866.1

Bertagni, M. B., Pacala, S. W., Paulot, F., & Porporato, A. (2022). Risk of the hydrogen economy for atmospheric methane. *Nature Communications*, *13*. https://doi.org/10.1038/s41467-022-35419-7

Chipperfield, M. P., Liang, Q., Strahan, S. E., Morgenstern, O., Dhomse, S. S., Abraham, N. L., Archibald, A. T., Bekki, S., Braesicke, P., Genova, G. D., Fleming, E. L., Hardiman, S. C., Iachetti, D., Jackman, C. H., Kinnison, D. E., Marchand, M., Pitari, G., Pyle, J. A., Rozanov, E., … Tummon, F. (2014). Multimodel estimates of atmospheric lifetimes of long-lived ozone-depleting substances: Present and future. *Journal of Geophysical Research*, *119*, 2555–2573. https://doi.org/10.1002/2013JD021097

Dessler, A. E., Hintsa, E. J., Weinstock, E. M., Anderson, J. G., & Chan, K. R. (1995). Mechanisms controlling water vapor in the lower stratosphere: "a tale of two stratospheres". *Journal of Geophysical Research: Atmospheres*, *100*(D11), 23167–23172. https://doi.org/10.1029/95JD02468

Dessler, A. E., Schoeberl, M. R., Wang, T., Davis, S. M., & Rosenlof, K. H. (2013). Stratospheric water vapor feedback. *Proceedings of the National Academy of Sciences of the United States of America*, *110*, 18087–18091. https://doi.org/10.1073/pnas.1310344110

Diallo, M. A., Ploeger, F., Hegglin, M. I., Ern, M., Grooß, J. U., Khaykin, S., & Riese, M. (2022). Stratospheric water vapour and ozone response to the quasi-biennial oscillation disruptions in 2016 and 2020. *Atmospheric Chemistry and Physics*, *22*, 14303–14321. https://doi.org/10.5194/acp-22-14303-2022

Dong, C., & Fu, Q. (2025). Stratosphere-troposphere exchange of water vapor based on observations and reanalyses [Preprint, posted May 27, 2025]. https://doi.org/10.22541/essoar.174835437.74618633/v1

Etminan, M., Myhre, G., Highwood, E. J., & Shine, K. P. (2016). Radiative forcing of carbon dioxide, methane, and nitrous oxide: A significant revision of the methane radiative forcing. *Geophysical Research Letters*, *43*, 12, 614–12, 623. https://doi.org/10.1002/2016GL071930

Flightpath 2050: Europe's vision for aviation – maintaining global leadership and serving society's needs. (2011). Publications Office. https://doi.org/https://doi.org/10.2777/50266

Frank, F., Jöckel, P., Gromov, S., & Dameris, M. (2018). Investigating the yield of h2o and h2 from methane oxidation in the stratosphere. *Atmospheric Chemistry and Physics*, *18*, 9955–9973. https://doi.org/10.5194/acp-18-9955-2018

Fueglistaler, S., Liu, Y. S., Flannaghan, T. J., Haynes, P. H., Dee, D. P., Read, W. J., Remsberg, E. E., Thomason, L. W., Hurst, D. F., Lanzante, J. R., & Bernath, P. F. (2013). The relation between atmospheric humidity and temperature trends for stratospheric water. *Journal of Geophysical Research Atmospheres*, *118*, 1052–1074. https://doi.org/10.1002/jgrd.50157

Fueglistaler, S., Bonazzola, M., Haynes, P. H., & Peter, T. (2005). Stratospheric water vapor predicted from the lagrangian temperature history of air entering the stratosphere in the tropics. *Journal of Geophysical Research D: Atmospheres*, *110*, 1–10. https://doi.org/10.1029/2004JD005516

Garny, H., Ploeger, F., Abalos, M., Bönisch, H., Castillo, A. E., von Clarmann, T., Diallo, M., Engel, A., Laube, J. C., Linz, M., Neu, J. L., Podglajen, A., Ray, E., Rivoire, L., Saunders, L. N., Stiller, G., Voet, F., Wagenhäuser, T., & Walker, K. A. (2024, December). Age of stratospheric air: Progress on processes, observations, and long-term trends. https://doi.org/10.1029/2023RG000832

Gettelman, A., Hegglin, M. I., Son, S. W., Kim, J., Fujiwara, M., Birner, T., Kremser, S., Rex, M., Añel, J. A., Akiyoshi, H., Austin, J., Bekki, S., Braesike, P., Brhl, C., Butchart, N., Chipperfield, M., Dameris, M., Dhomse, S., Garny, H., … Tian, W. (2010). Multimodel assessment of the upper troposphere and lower stratosphere: Tropics and global trends. *Journal of Geophysical Research Atmospheres*, *115*. https://doi.org/10.1029/2009JD013638

Grewe, V., Frömming, C., Matthes, S., Brinkop, S., Ponater, M., Dietmüller, S., Jöckel, P., Garny, H., Tsati, E., Dahlmann, K., Søvde, O. A., Fuglestvedt, J., Berntsen, T. K., Shine, K. P., Irvine, E. A., Champougny, T., & Hullah, P. (2014). Aircraft routing with minimal climate impact: The react4c climate cost function modelling approach (v1.0). *Geoscientific Model Development*, *7*, 175–201. https://doi.org/10.5194/gmd-7-175-2014

Grewe, V., & Stenke, A. (2008). Airclim: An efficient tool for climate evaluation of aircraft technology. *Atmospheric Chemistry and Physics*, *8*, 4621–4639. https://doi.org/10.5194/acp-8-4621-2008

Grewe, V., Rao, A. G., Grönstedt, T., Xisto, C., Linke, F., Melkert, J., Middel, J., Ohlenforst, B., Blakey, S., Christie, S., Matthes, S., & Dahlmann, K. (2021). Evaluating the climate impact of aviation emission scenarios towards the paris agreement including covid-19 effects. *Nature Communications*, *12*. https://doi.org/10.1038/s41467-021-24091-y

Gunter, F. A. (2024, December). *The climate impact of hydrogen leakage in aviation* (tech. rep.). Delft University of Technology. http://repository.tudelft.nl/.

Hall, T. M., & Plumb, R. A. (1994). Age as a diagnostic of stratospheric transport. *Journal of Geophysical Research*, *99*, 1059–1070. https://doi.org/10.1029/93JD03192

Hall, T. M., & Waugh, D. W. (2000). Stratospheric residence time and its relationship to mean age. *Journal of Geophysical Research Atmospheres*, *105*, 6773–6782. https://doi.org/10.1029/1999JD901096

Hegglin, M. I., Plummer, D. A., Shepherd, T. G., Scinocca, J. F., Anderson, J., Froidevaux, L., Funke, B., Hurst, D., Rozanov, A., Urban, J., Clarmann, T. V., Walker, K. A., Wang, H. J., Tegtmeier, S., & Weigel, K. (2014). Vertical structure of stratospheric water vapour trends derived from merged satellite data. *Nature Geoscience*, *7*, 768–776. https://doi.org/10.1038/NGEO2236

Hoffmann, L., & Spang, R. (2022). An assessment of tropopause characteristics of the era5 and era-interim meteorological reanalyses. *Atmospheric Chemistry and Physics*, *22*(6), 4019–4046. https://doi.org/10.5194/acp-22-4019-2022

Holzer, M., Orbe, C., & Primeau, F. W. (2012). Stratospheric mean residence time and mean age on the tropopause: Connections and implications for observational constraints. *Journal of Geophysical Research Atmospheres*, *117*. https://doi.org/10.1029/2012JD017547

Houghton, J. T., Jenkins, G. J., & Ephraums, J. J. (Eds.). (1990). *Climate change: The ipcc scientific assessment*. Cambridge University Press.

IPCC. (2001). *Climate change 2001: The scientific basis* [Third Assessment Report]. Cambridge University Press. https://archive.ipcc.ch/ipccreports/tar/wg1/index.php?idp=224

IPCC. (2013). *Climate change 2013: The physical science basis* [Contribution of Working Group I to the Fifth Assessment Report]. Cambridge University Press. https://www.ipcc.ch/report/ar5/wg1/

Kirschke, S., Bousquet, P., Ciais, P., Saunois, M., Canadell, J. G., Dlugokencky, E. J., Bergamaschi, P., Bergmann, D., Blake, D. R., Bruhwiler, L., Cameron-Smith, P., Castaldi, S., Chevallier, F., Feng, L., Fraser, A., Heimann, M., Hodson, E. L., Houweling, S., Josse, B., … Zeng, G. (2013, October). Three decades of global methane sources and sinks. https://doi.org/10.1038/ngeo1955

Klöwer, M., Allen, M. R., Lee, D. S., Proud, S. R., Gallagher, L., & Skowron, A. (2021). Quantifying aviation's contribution to global warming. *Environmental Research Letters*, *16*(10), 104027. https://doi.org/10.1088/1748-9326/ac286e

le Texier, H., Solomon, S., & Garcia, R. R. (1988). The role of molecular hydrogen and methane oxidation in the water vapour budget of the stratosphere. *Quarterly Journal of the Royal Meteorological Society*, *114*, 281–295. https://doi.org/10.1002/qj.49711448002

Lee, D. S., Fahey, D. W., Skowron, A., Allen, M. R., Burkhardt, U., Chen, Q., Doherty, S. J., Freeman, S., Forster, P. M., Fuglestvedt, J., Gettelman, A., León, R. R. D., Lim, L. L., Lund, M. T., Millar, R. J., Owen, B., Penner, J. E., Pitari, G., Prather, M. J., … Wilcox, L. J. (2021). The contribution of global aviation to anthropogenic climate forcing for 2000 to 2018. *Atmospheric Environment*, *244*. https://doi.org/10.1016/j.atmosenv.2020.117834

Megill, L., Deck, K., & Grewe, V. (2024). Alternative climate metrics to the global warming potential are more suitable for assessing aviation non-co2 effects. *Communications Earth and Environment*, *5*. https://doi.org/10.1038/s43247-024-01423-6

Meinshausen, M., Nicholls, Z. R., Lewis, J., Gidden, M. J., Vogel, E., Freund, M., Beyerle, U., Gessner, C., Nauels, A., Bauer, N., Canadell, J. G., Daniel, J. S., John, A., Krummel, P. B., Luderer, G., Meinshausen, N., Montzka, S. A., Rayner, P. J., Reimann, S., … Wang, R. H. (2020). The

shared socio-economic pathway (ssp) greenhouse gas concentrations and their extensions to 2500. *Geoscientific Model Development*, *13*, 3571–3605. https://doi.org/10.5194/gmd-13-3571-2020

Myhre, G., Shindell, D., Bréon, F.-M., Collins, W., Fuglestvedt, J., Huang, J., Koch, D., Lamarque, J.-F., Lee, D., Mendoza, B., Nakajima, T., Robock, A., Stephens, G., Takemura, T., & Zhang, H. (2013). Anthropogenic and natural radiative forcing. In T. Stocker, D. Qin, G.-K. Plattner, M. Tignor, S. Allen, J. Boschung, A. Nauels, Y. Xia, V. Bex, & P. Midgley (Eds.), *Climate change 2013: The physical science basis. contribution of working group i to the fifth assessment report of the intergovernmental panel on climate change* (pp. 659–740). Cambridge University Press. https://www.ipcc.ch/report/ar5/wg1/chapter-8-anthropogenic-and-natural-radiative-forcing/

Myhre, G., Kvalevåg, M., Rädel, G., Cook, J., Shine, K. P., Clark, H., Karcher, F., Markowicz, K., Kardas, A., Wolkenberg, P., Balkanski, Y., Ponater, M., Forster, P., Rap, A., & Leon, R. R. D. (2009). Intercomparison of radiative forcing calculations of stratospheric water vapour and contrails. *Meteorologische Zeitschrift*, *18*, 585–596. https://doi.org/10.1127/0941-2948/2009/0411

Myhre, G., Nilsen, J. S., Gulstad, L., Shine, K. P., Rognerud, B., & Isaksen, I. S. (2007). Radiative forcing due to stratospheric water vapour from ch4 oxidation. *Geophysical Research Letters*, *34*. https://doi.org/10.1029/2006GL027472

Nowack, P., Ceppi, P., Davis, S. M., Chiodo, G., Ball, W., Diallo, M. A., Hassler, B., Jia, Y., Keeble, J., & Joshi, M. (2023). Response of stratospheric water vapour to warming constrained by satellite observations. *Nature Geoscience*, *16*, 577–583. https://doi.org/10.1038/s41561-023-01183-6

Oman, L., Waugh, D. W., Pawson, S., Stolarski, R. S., & Nielsen, J. E. (2008). Understanding the changes of stratospheric water vapor in coupled chemistry-climate model simulations. *Journal of the Atmospheric Sciences*, *65*, 3278–3291. https://doi.org/10.1175/2008JAS2696.1

Park, J. H., III, J. M. R., Gordley, L. L., Drayson, S. R., Benner, D. C., McInerney, J. M., Gunson, M. R., Toon, G. C., Sen, B., Blavier, J.-F., Webster, C. R., Zipf, E. C., Erdman, P., Schmidt, U., & Schiller, C. (1996). Validation of halogen occultation experiment ch4 measurements from the uars. *Journal of Geophysical Research: Atmospheres*, *101*(D6), 10183–10203. https://doi.org/10.1029/95JD02736

Paulot, F., Paynter, D., Naik, V., Malyshev, S., Menzel, R., & Horowitz, L. W. (2021). Global modeling of hydrogen using gfdl-am4.1: Sensitivity of soil removal and radiative forcing. *International Journal of Hydrogen Energy*, *46*, 13446–13460. https://doi.org/10.1016/j.ijhydene.2021.01.088

Penner, J., Lister, D., Griggs, D., Dokken, D., & McFarland, M. (Eds.). (1999). *Ipcc special report: Aviation and the global atmosphere* [Prepared in collaboration with the Scientific Assessment Panel to the Montreal Protocol on Substances that Deplete the Ozone Layer]. Cambridge University Press.

Pletzer, J. (2024). The climate impact of hypersonic transport. *Dissertation (TU Delft), Delft University of Technology*. https://doi.org/10.4233/uuid:39acca9a-53ba-4b9c-b9c0-b6c99f552e25

Randel, W., & Park, M. (2019). Diagnosing observed stratospheric water vapor relationships to the cold point tropical tropopause. *Journal of Geophysical Research: Atmospheres*, *124*, 7018–7033. https://doi.org/10.1029/2019JD030648

Revell, L. E., Stenke, A., Rozanov, E., Ball, W., Lossow, S., & Peter, T. (2016). The role of methane in projections of 21st century stratospheric water vapour. *Atmospheric Chemistry and Physics*, *16*, 13067–13080. https://doi.org/10.5194/acp-16-13067-2016

Rieger, V. (2018). A new method to assess the climate effect of mitigation strategies for road traffic. *Dissertation (TU Delft), Delft University of Technology*. https://doi.org/10.4233/uuid:cc96a7c7-1ec7-449a-84b0-2f9a342a5be5

Sand, M., Skeie, R. B., Sandstad, M., Krishnan, S., Myhre, G., Bryant, H., Derwent, R., Hauglustaine, D., Paulot, F., Prather, M., & Stevenson, D. (2023). A multi-model assessment of the global warming potential of hydrogen. *Communications Earth and Environment*, *4*. https://doi.org/10.1038/s43247-023-00857-8

Schumann, U. (1997). *The impact of nitrogen oxides emissions from aircraft upon the atmosphere at flight altitudes-results from the aeronox project* (tech. rep.).

Shine, K. P., Fuglestvedt, J. S., Hailemariam, K., & Stuber, N. (2005). Alternatives to the global warming potential for comparing climate impacts of emissions of greenhouse gases. *Climatic Change*, *68*(3), 281–302. https://doi.org/10.1007/s10584-005-1146-9

Skeie, R. B., Sandstad, M., Krishnan, S., Myhre, G., & Sand, M. (2025). Sensitivity of climate effects of hydrogen to leakage size, location, and chemical background. *Atmospheric Chemistry and Physics*, *25*, 4929–4942. https://doi.org/10.5194/acp-25-4929-2025

Solomon, S., Rosenlof, K. H., Portmann, R. W., Daniel, J. S., Davis, S. M., Sanford, T. J., & Plattner, G. K. (2010). Contributions of stratospheric water vapor to decadal changes in the rate of global warming. *Science*, *327*, 1219–1223. https://doi.org/10.1126/science.1182488

Stevenson, D. S., Dentener, F. J., Schultz, M. G., Ellingsen, K., van Noije, T. P. C., Wild, O., Zeng, G., Amann, M., Atherton, C. S., Bell, N., Bergmann, D. J., Bey, I., Butler, T., Cofala, J., Collins, W. J., Derwent, R. G., Doherty, R. M., Drevet, J., Eskes, H. J., … Szopa, S. (2006). Multimodel ensemble simulations of present-day and near-future tropospheric ozone. *Journal of Geophysical Research: Atmospheres*, *111*(D8). https://doi.org/https://doi.org/10.1029/2005JD006338

Tissier, A.-S., & Legras, B. (2016). Convective sources of trajectories traversing the tropical tropopause layer. *Atmospheric Chemistry and Physics*, *16*(5), 3383–3398. https://doi.org/10.5194/acp-16-3383-2016

Völk, S., Yamashita, H., Megill, L., Dahlmann, K., & Grewe, V. (2026). *Openairclim v0.11.0: A framework for assessing the climate impact of aviation emissions* [Manuscript in preparation].

Voulgarakis, A., Naik, V., Lamarque, J. F., Shindell, D. T., Young, P. J., Prather, M. J., Wild, O., Field, R. D., Bergmann, D., Cameron-Smith, P., Cionni, I., Collins, W. J., Dalsøren, S. B., Doherty, R. M., Eyring, V., Faluvegi, G., Folberth, G. A., Horowitz, L. W., Josse, B., … Zeng, G. (2013). Analysis of present day and future oh and methane lifetime in the accmip simulations. *Atmospheric Chemistry and Physics*, *13*, 2563–2587. https://doi.org/10.5194/acp-13-2563-2013

Warwick, N., Griffiths, P., Keeble, J., Archibald, A., & Pyle, J. (2022). *Atmospheric implications of increased hydrogen use* (tech. rep.).

Waugh, D. W., & Hall, T. M. (2002). Age of stratospheric air: Theory, observations, and models. *Reviews of Geophysics*, *40*, 1-1-1–26. https://doi.org/10.1029/2000RG000101

Wilcox, L. J., Shine, K. P., & Hoskins, B. J. (2012). Radiative forcing due to aviation water vapour emissions. *Atmospheric Environment*, *63*, 1–13. https://doi.org/10.1016/j.atmosenv.2012.08.072

Winterstein, F., & Jöckel, P. (2021). Methane chemistry in a nutshell-the new submodels ch4 (v1.0) and trsync (v1.0) in messy (v2.54.0). *Geoscientific Model Development*, *14*, 661–674. https://doi.org/10.5194/gmd-14-661-2021

A

Assessment of Aviation-Induced Changes in Stratospheric Water Vapour Transport

In this appendix, some additional calculations are done to support the decision to omit a module in OAC that takes the effect of aviation emissions on the water vapour transport from the troposphere to the stratosphere into account.

Aviation's Impact on Stratospheric Water Vapour Entry Concentration

Aviation influences global warming by emitting CO_2 and other greenhouse gases. Klöwer et al. (2021) estimate the warming due to aviation at 0.1 °C at 2050. When this 0.1 °C is combined with the increase in entry water vapour of 0.31 ppmv K^{-1} from Nowack et al. (2023), an increase in entry H_2O of 0.031 ppmv is caused by aviation in 2050. Standard air entry values are estimated to be between 3 and 5 ppmv (Fueglistaler et al., 2005; Hegglin et al., 2014). This means that the increase in H_2O transported from the troposphere to the stratosphere due to aviation will be about 1-2%. This 1-2% increase in H_2O entry concentration is for all warming of aviation since aviation started early 20th century.

To get some insight into future perspectives, the data from Klöwer et al. (2021) is used to estimate the global warming due to aviation emissions from 2019 to 2050. Klöwer et al. (2021) states that the global warming due to aviation is 0.04K at 2019 and 0.1K in 2050 This causes the temperature to increase by 0.06K from 2019 to 2050. Combining with the value of 0.31 ppmv K^{-1} from Nowack et al. (2023), the entry water vapour concentration increases by 0.0186 ppmv. linearizing this increase to an increase per year yields an increase in water vapour entry concentration of 0.6 ppbv yr^{-1}.

Conversion to Stratospheric Water Vapour Mass Flux

Relating the volume ratio to a mass ratio with the use of molar masses of water and air, the 0.6 ppbv yr^{-1} increase can be translated to a mass ratio of 3.7 $\times$ 10^{-10} Tg(SWV) Tg(air)$^{-1}$ yr^{-1}. When relating this additional input H_2O with the total mass entering the stratosphere from the troposphere of about 6-9 10^8 Tg yr^{-1} (Tissier & Legras, 2016), an additional amount of SWV of 0.22-0.34 Tg yr^{-1} enters the stratosphere due to aviation-induced warming between 2019 and 2050.

Interpretation, and Implications for Model Scope

The estimated increase in stratospheric entry water vapour of approximately 0.0186 ppmv over the period 2019-2050 is negligible compared to the uncertainty bounds reported in the literature. Typical entry mixing ratios are estimated to range between 3–5 ppmv (Fueglistaler et al., 2005), such that the aviation-induced perturbation represents less than 0.5% of the background value. This magnitude is small compared to both interannual variability and observational uncertainty in stratospheric water vapour entry concentrations.

Expressed in terms of mass flux, the additional 0.22-0.34 Tg yr^{-1} of stratospheric water vapour attributable to aviation-induced warming is negligible relative to total annual troposphere–stratosphere water vapour transport, which is estimated to be on the order of 1.1–2.8 Pg yr^{-1} (Fueglistaler et al., 2005; Tissier & Legras, 2016) or approximately 2.2 Pg yr^{-1} according to Dong and Fu (2025). On an annual basis, the aviation-induced contribution therefore amounts to roughly 0.02% of the total flux. While the cumulative contribution over 30 years would correspond to approximately 0.5% of the yearly total stratospheric water vapour input, this comparison is not physically consistent, as stratospheric water vapour is continuously removed as well. As the background stratospheric water vapour burden increases, removal rates also increase, further limiting the persistence of any small perturbation.

Several limitations of this assessment should be noted. The analysis is based on order-of-magnitude estimates, relying on simplified representations of H_2O transport from the troposphere to the stratosphere. Uncertainties in estimates of total stratospheric water vapour transport are substantial, commonly on the order of 50% or more, and therefore exceed the magnitude of the aviation-induced signal by more than two orders of magnitude. As a result, the perturbation estimated here would not be distinguishable from natural variability or structural uncertainty in current models.

In conclusion, explicitly modelling this feedback would not meaningfully improve the representation of aviation-induced climate effects. The exclusion of this pathway from the OpenAirClim framework is therefore a quantitatively justified scope decision and does not affect the robustness of the scenario and uncertainty analyses presented in this thesis.

B

Supplementary Scenario Results

This appendix presents additional model output generated during the scenario analysis (chapter 6). The results shown here are produced as part of the modelling workflow but are not used in the main body of the thesis, as they do not directly contribute to the research questions. They are included for completeness and to document the full range of outputs produced by the model.

All figures in this appendix follow a consistent visual convention. Colours indicate aviation emission scenarios, based on the publication from Grewe et al. (2021). Blue represents Business-as-Usual (BAU), red represents Current Technology (CurTec), grey represents FlightPath 2050 (FP2050), and purple represents FlightPath 2050 continuous (FP2050cont). Line styles indicate the background socio-economic pathways (SSPs): solid lines correspond to SSP1-1.9, dashed lines to SSP2-4.5, dotted lines to SSP3-7.0, and dash-dotted lines to SSP4-6.0.

In section B.1, section B.2, section B.3, and section B.4, the figures related to RF, dT, GWP20, and ATR20 are shown, respectively.

B.1. Radiative Forcing (RF)

This section presents radiative forcing (RF) results for all combinations of aviation emission scenarios and SSP background pathways. These figures are provided for completeness and to illustrate the full set of RF outputs generated by the model.

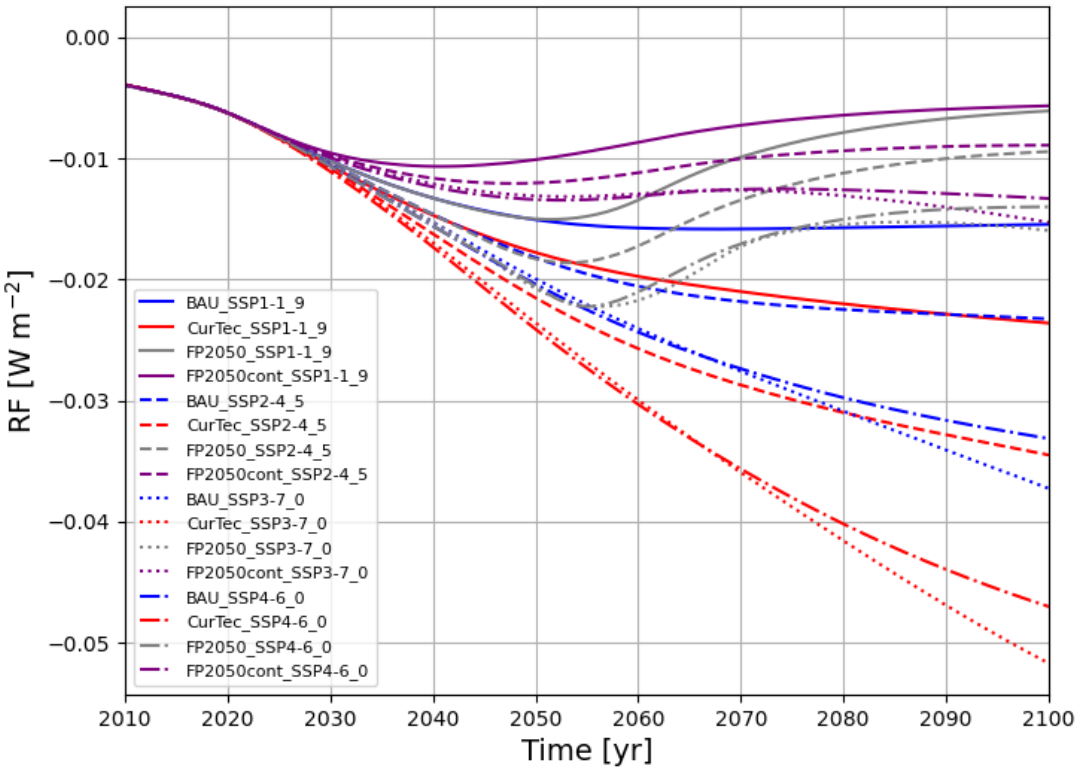

Figure B.1: Radiative forcing for the different scenarios with different backgrounds. Colours indicate aviation emission scenarios, blue represents Business-as-Usual (BAU), red represents Current Technology (CurTec), grey represents FlightPath 2050 (FP2050), and purple represents FlightPath 2050 continuous (FP2050cont). Line styles indicate the background socio-economic pathways (SSPs): solid lines correspond to SSP1-1.9, dashed lines to SSP2-4.5, dotted lines to SSP3-7.0, and dash-dotted lines to SSP4-6.0.

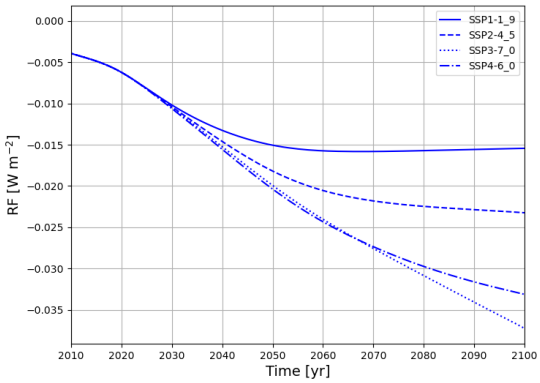

(a) RF BAU

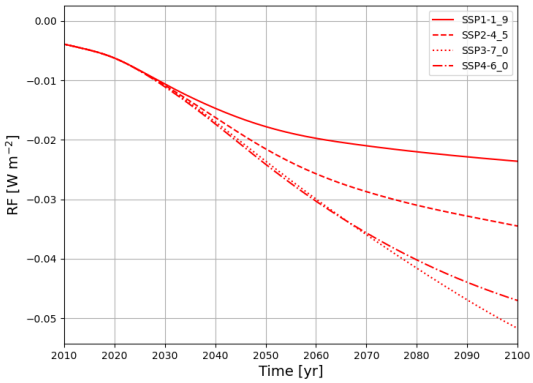

(b) RF CurTec

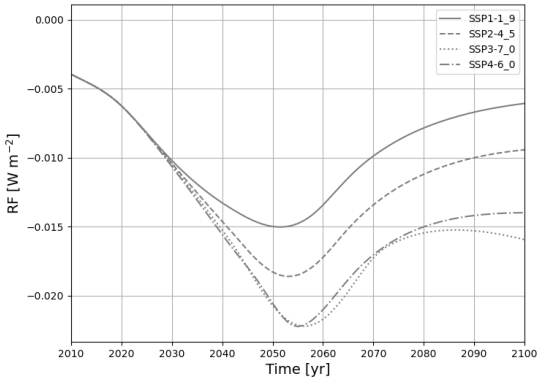

(c) RF FP2050

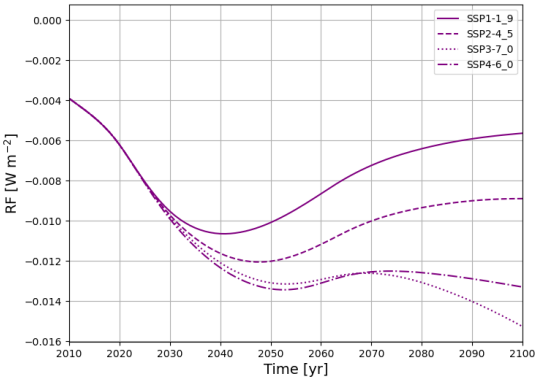

(d) RF FP2050cont

Figure B.2: The same results as in Figure B.1 are presented here, but separated by scenario for clarity.

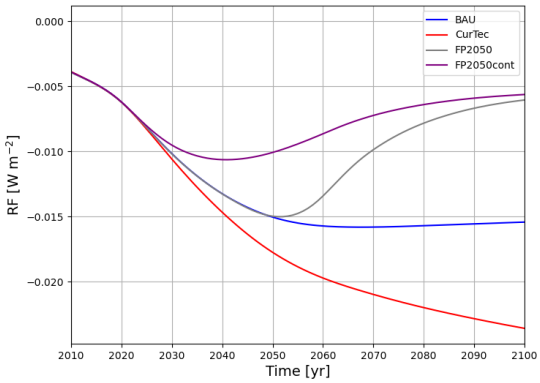

(a) RF SSP1-1.9

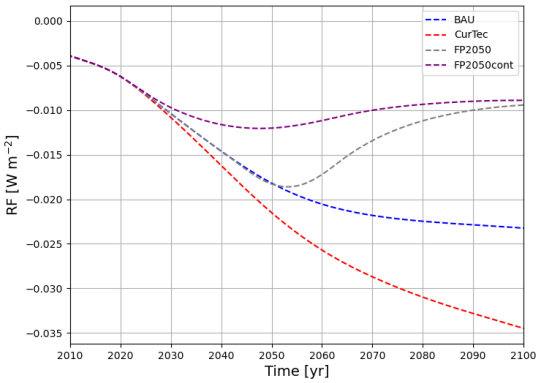

(b) RF SSP2-4.5

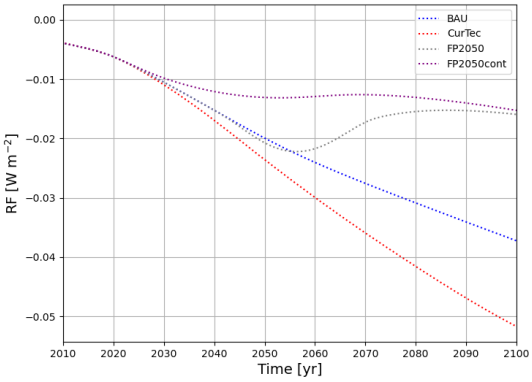

(c) RF SSP3-7.0

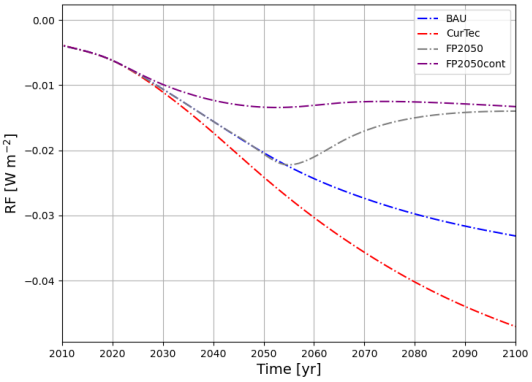

(d) RF SSP4-6.0

Figure B.3: The same results as in Figure B.1 are presented here, but separated by background scenario for clarity.

B.2. Temperature Change (dT)

This section presents the global mean temperature change (dT) results for all combinations of aviation emission scenarios and SSP background pathways. These figures are provided for completeness and to illustrate the full set of dT outputs generated by the model.

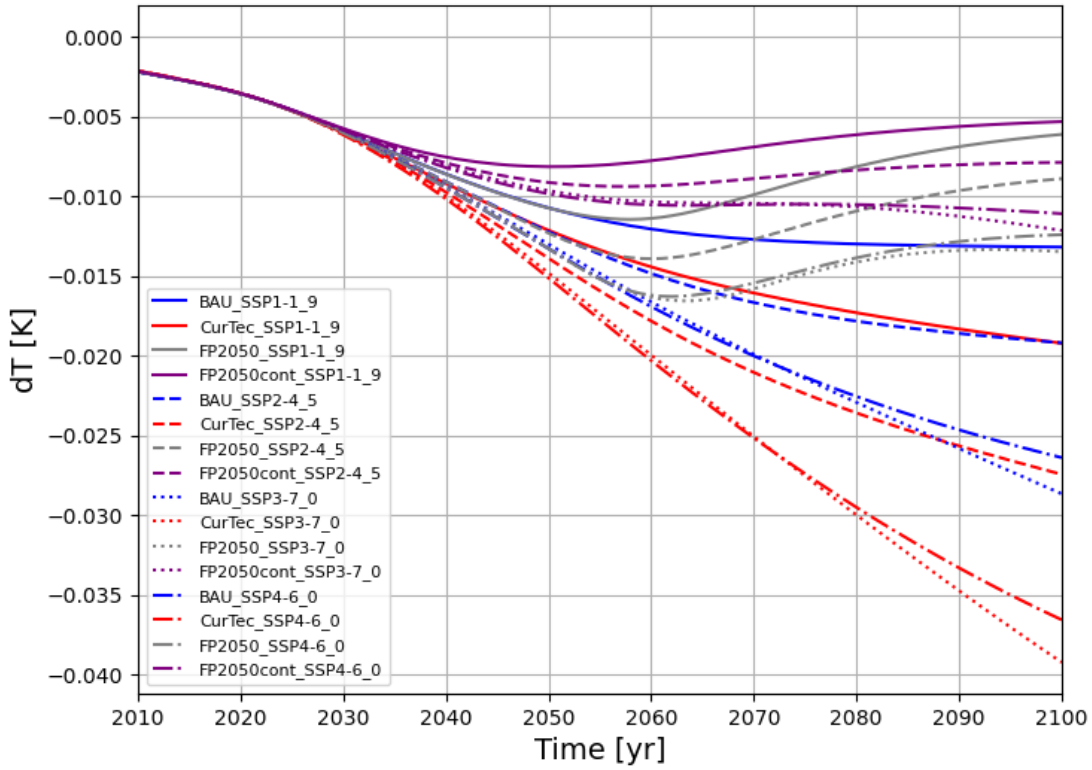

Figure B.4: Temperature change for the different scenarios with different backgrounds. Colours indicate aviation emission scenarios, blue represents Business-as-Usual (BAU), red represents Current Technology (CurTec), grey represents FlightPath 2050 (FP2050), and purple represents FlightPath 2050 continuous (FP2050cont). Line styles indicate the background socio-economic pathways (SSPs): solid lines correspond to SSP1-1.9, dashed lines to SSP2-4.5, dotted lines to SSP3-7.0, and dash-dotted lines to SSP4-6.0.

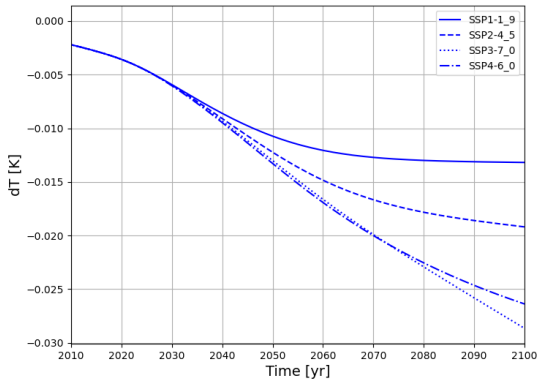

(a) dT BAU

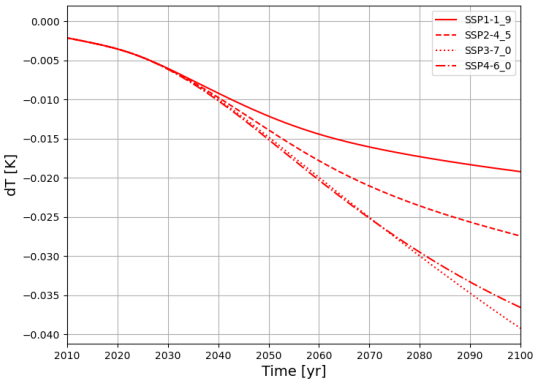

(b) dT CurTec

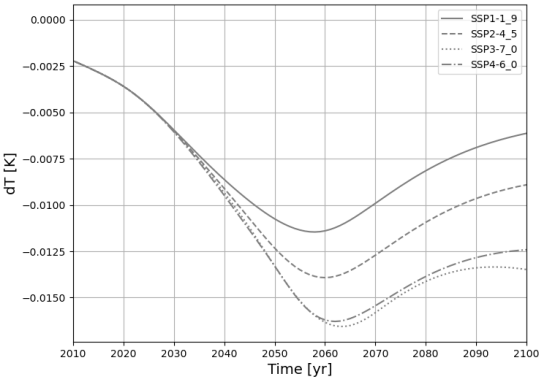

(c) dT FP2050

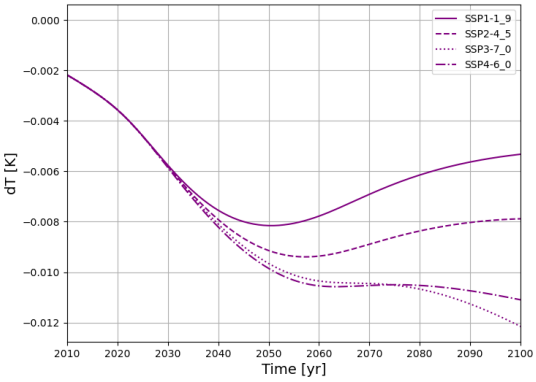

(d) dT FP2050cont

Figure B.5: The same results as in Figure B.4 are presented here, but separated by scenario for clarity.

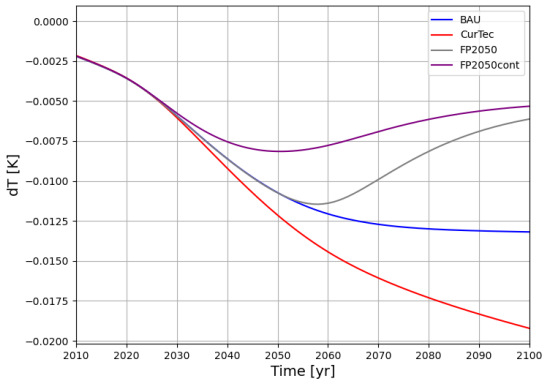

(a) dT SSP1-1.9

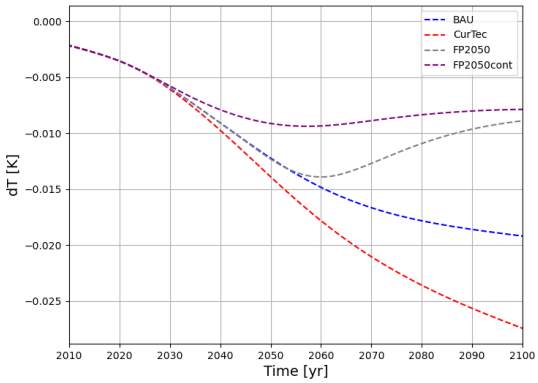

(b) dT SSP2-4.5

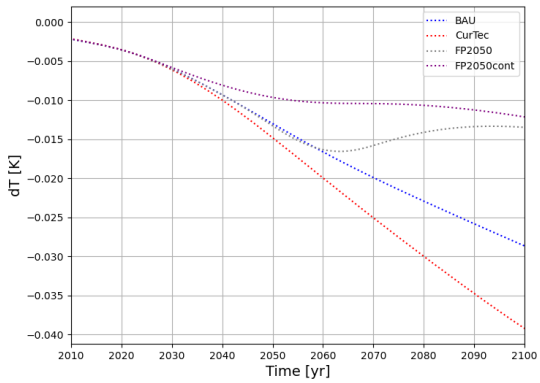

(c) dT SSP3-7.0

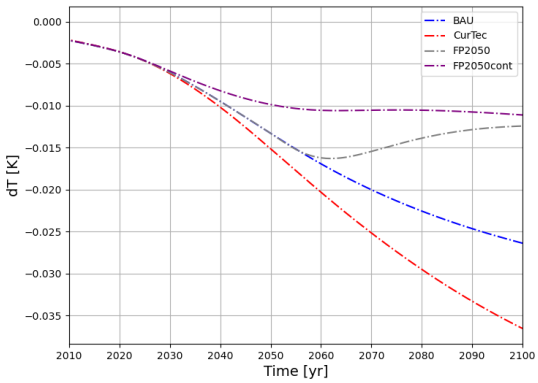

(d) dT SSP4-6.0

Figure B.6: The same results as in Figure B.4are presented here, but separated by background scenario for clarity.

B.3. Global Warming Potential (GWP)

This section presents the GWP20 values derived from the simulated radiative forcing time series for all combinations of aviation emission scenarios and SSP background pathways. These figures are provided for completeness and to illustrate the full set of RF outputs generated by the model.

For each evaluation year x, the climate impact is integrated over the subsequent 20 years, i.e. from x to x + 20, consistent with the definition of GWP as a forward-looking metric with a fixed time horizon. As the model simulations extend until 2100, GWP20 values can only be computed up to 2080, beyond which the required 20-year integration window would exceed the available data. The resulting GWP20 value obtained for each year is assigned to the corresponding evaluation year x and plotted accordingly in Figure B.7.

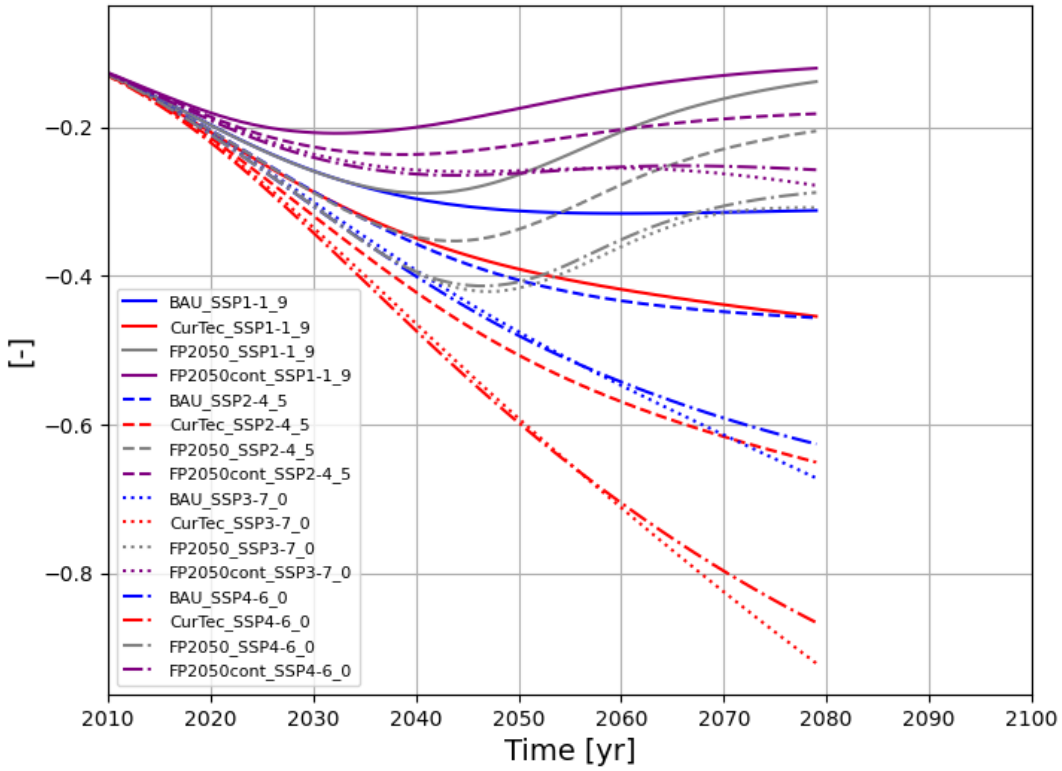

Figure B.7: The global warming potential for a time horizon of twenty years is displayed here for the different scenarios with different backgrounds. Colours indicate aviation emission scenarios, blue represents Business-as-Usual (BAU), red represents Current Technology (CurTec), grey represents FlightPath 2050 (FP2050), and purple represents FlightPath 2050 continuous (FP2050cont). Line styles indicate the background socio-economic pathways (SSPs): solid lines correspond to SSP1-1.9, dashed lines to SSP2-4.5, dotted lines to SSP3-7.0, and dash-dotted lines to SSP4-6.0.

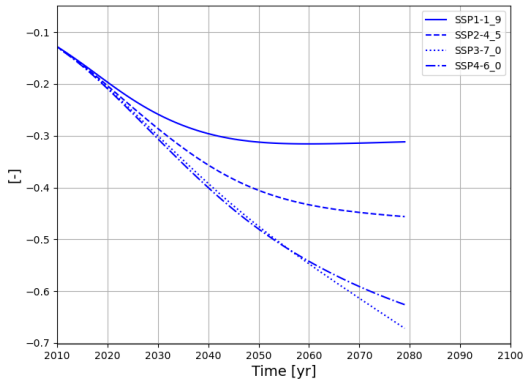

(a) GWP20 BAU

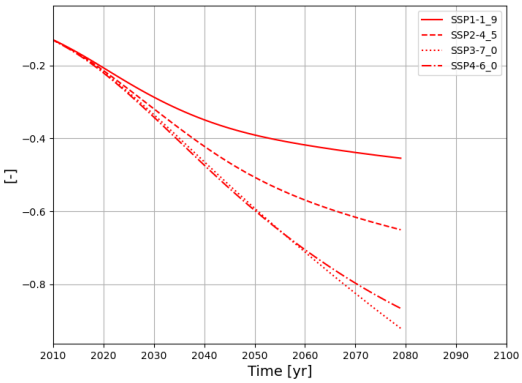

(b) GWP20 CurTec

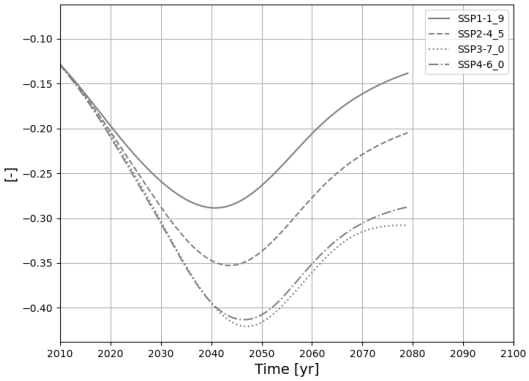

(c) GWP20 FP2050

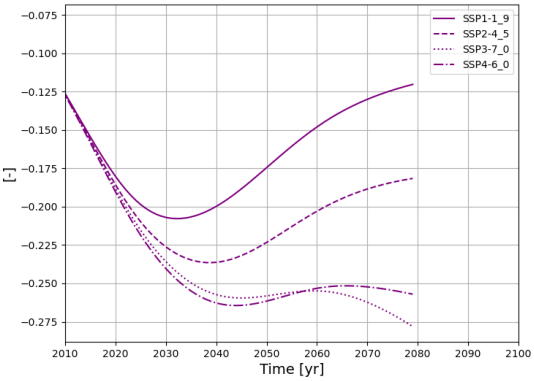

(d) GWP20 FP2050cont

Figure B.8: The same results as in Figure B.7 are presented here, but separated by scenario for clarity.

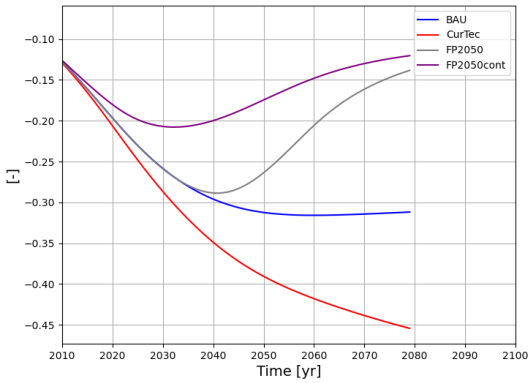

(a) GWP20 SSP1-1.9

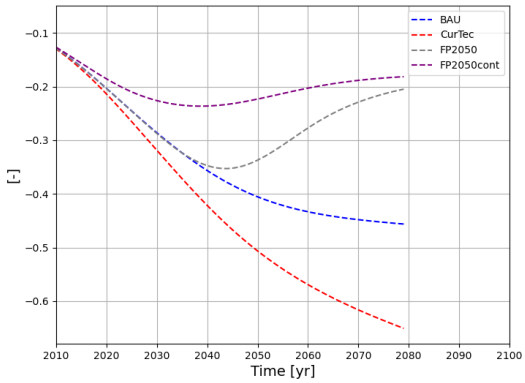

(b) GWP20 SSP2-4.5

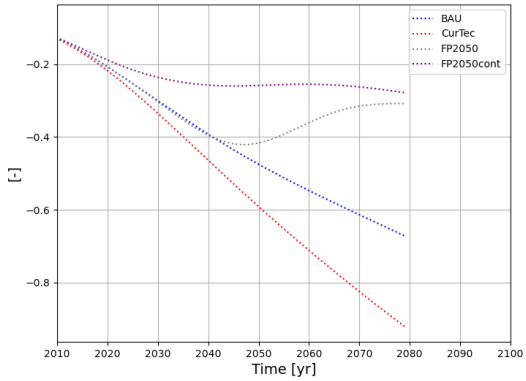

(c) GWP20 SSP3-7.0

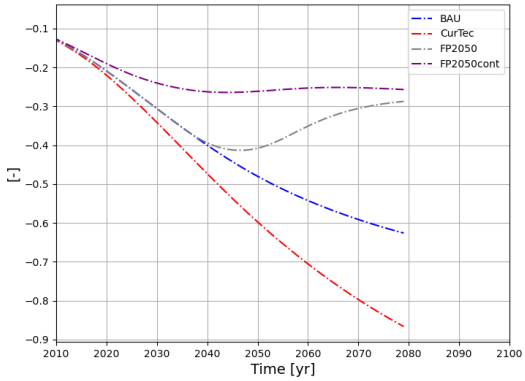

(d) GWP20 SSP4-6.0

Figure B.9: The same results as in Figure B.7 are presented here, but separated by background scenario for clarity.

B.4. Average Temperature Response (ATR)

This section presents the ATR20 values derived from the simulated radiative forcing time series for all combinations of aviation emission scenarios and SSP background pathways. These figures are provided for completeness and to illustrate the full set of RF outputs generated by the model.

For each evaluation year x, the climate impact is integrated over the subsequent 20 years, i.e. from x to x + 20, consistent with the definition of ATR as a forward-looking metric with a fixed time horizon. As the model simulations extend until 2100, ATR20 values can only be computed up to 2080, beyond which the required 20-year integration window would exceed the available data. The resulting ATR20 value obtained for each year is assigned to the corresponding evaluation year x and plotted accordingly in Figure B.10.

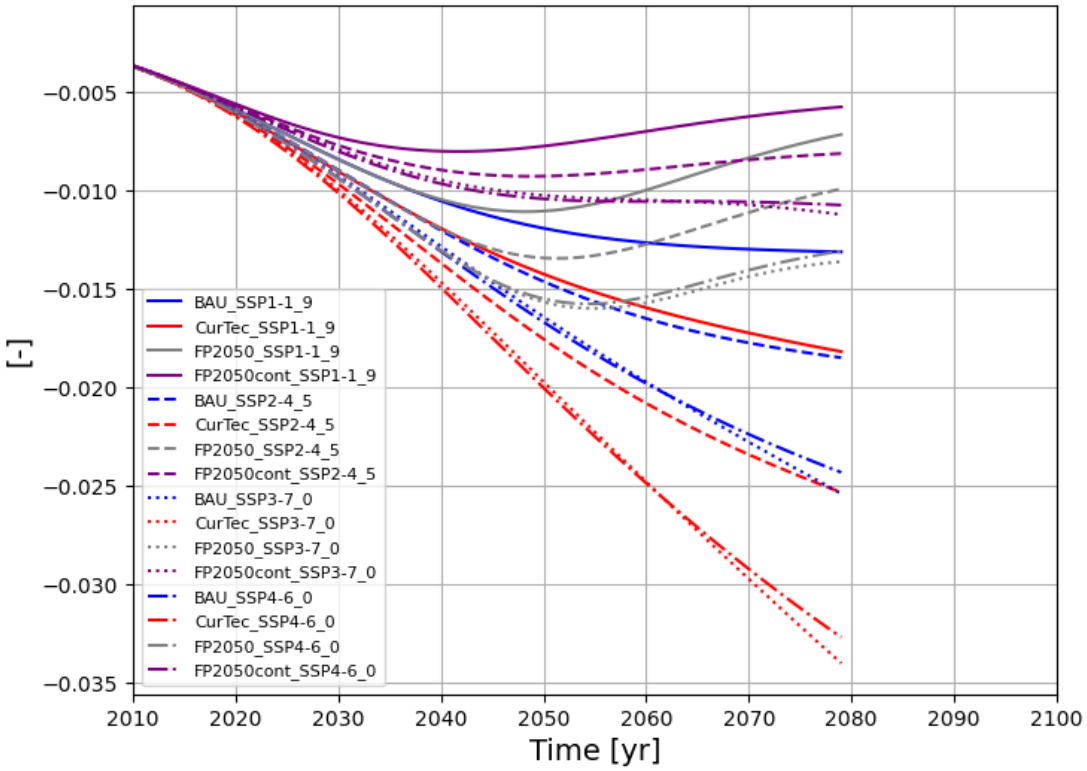

Figure B.10: The average temperature response for a time horizon of twenty years is displayed here for the different scenarios with different backgrounds. Colours indicate aviation emission scenarios, blue represents Business-as-Usual (BAU), red represents Current Technology (CurTec), grey represents FlightPath 2050 (FP2050), and purple represents FlightPath 2050 continuous (FP2050cont). Line styles indicate the background socio-economic pathways (SSPs): solid lines correspond to SSP1-1.9, dashed lines to SSP2-4.5, dotted lines to SSP3-7.0, and dash-dotted lines to SSP4-6.0.

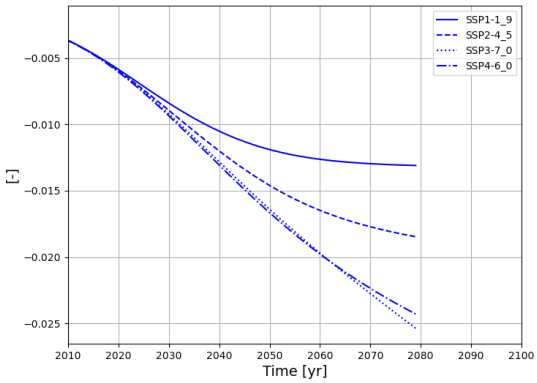

(a) ATR20 BAU

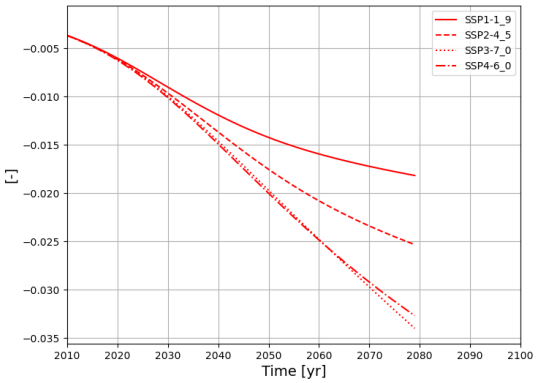

(b) ATR20 CurTec

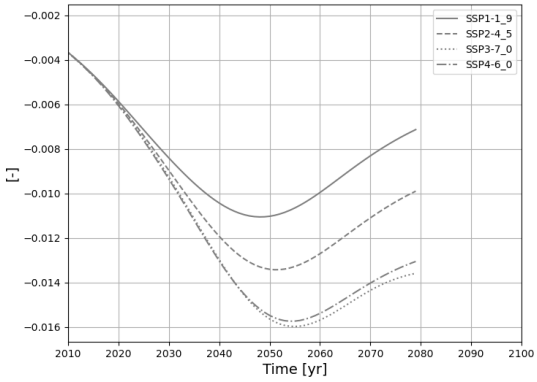

(c) ATR20 FP2050

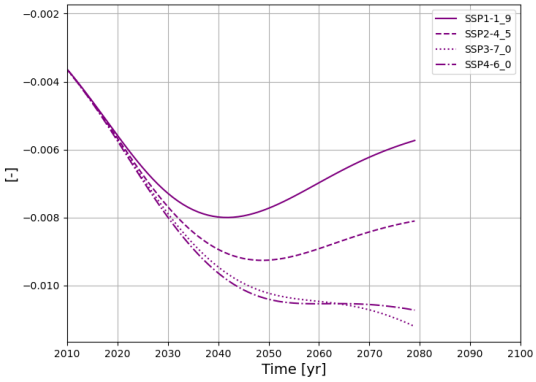

(d) ATR20 FP2050cont

Figure B.11: The same results as in Figure B.10 are presented here, but separated by scenario for clarity.

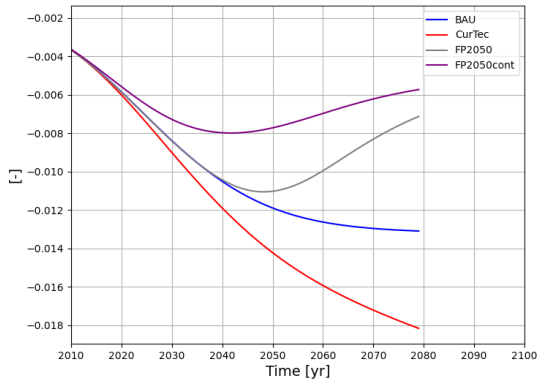

(a) ATR20 SSP1-1.9

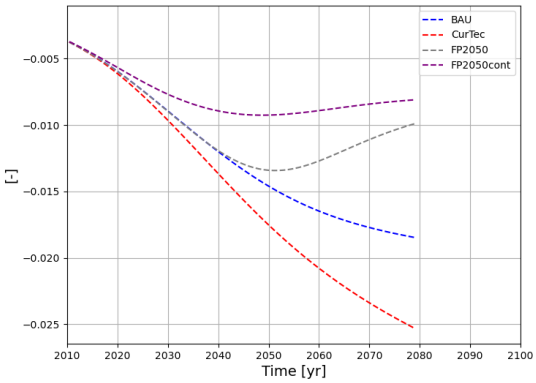

(b) ATR20 SSP2-4.5

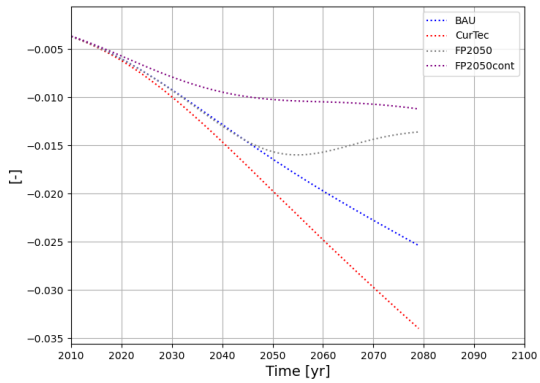

(c) ATR20 SSP3-7.0

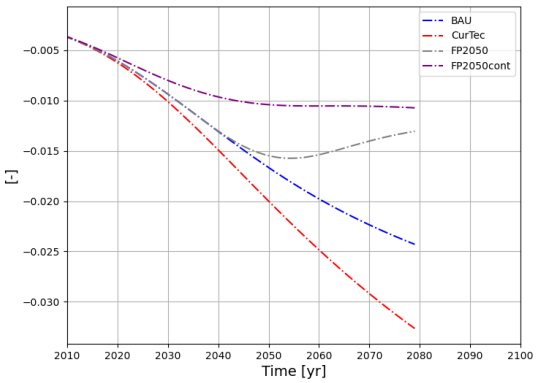

(d) ATR20 SSP4-6.0

Figure B.12: The same results as in Figure B.10 are presented here, but separated by background scenario for clarity.